Accepted Manuscript

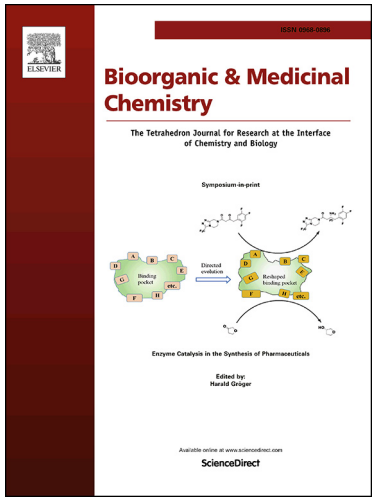

Synthesis, antiproliferative and apoptosis induction potential activities of novel Bis(indolyl)hydrazide-hydrazone derivatives

Reddymasu Sreenivasulu, Kotthireddy Thirumal Reddy, Pombala Sujitha, C. Ganesh Kumar, Rudraraju Ramesh Raju

PII: S0968-0896(18)31799-1
DOI: https://doi.org/10.1016/j.bmc.2019.02.002
Reference: BMC 14738

To appear in: *Bioorganic & Medicinal Chemistry*

Received Date: 19 October 2018
Revised Date: 29 January 2019
Accepted Date: 1 February 2019

Please cite this article as: Sreenivasulu, R., Reddy, K.T., Sujitha, P., Kumar, C.G., Raju, R.R., Synthesis, antiproliferative and apoptosis induction potential activities of novel Bis(indolyl)hydrazide-hydrazone derivatives, *Bioorganic & Medicinal Chemistry* (2019), doi: https://doi.org/10.1016/j.bmc.2019.02.002

Synthesis, antiproliferative and apoptosis induction potential activities of novel Bis(indolyl)hydrazide-hydrazone derivatives

Reddymasu Sreenivasulu,[a] Kotthireddy Thirumal Reddy,[a] Pombala Sujitha,[b] C. Ganesh Kumar,[b#] and Rudraraju Ramesh Raju[a]*

[1]*Department of Chemistry, Acharya Nagarjuna University, Nagarjuna Nagar – 522 510, Andhra Pradesh, India.*

[2]*Medicinal Chemistry and Pharmacology Division, CSIR-Indian Institute of Chemical Technology, Uppal Road, Tarnaka, Hyderabad 500007, Telangana, India.*

Abstract:

In recent years, indole-indazolyl hydrazide-hydrazone derivatives with strong cell growth inhibition and apoptosis induction characteristics are being strongly screened for their cancer chemo-preventive potential. In the present study, N-methyl and N,N-dimethyl bis(indolyl)hydrazide-hydrazone analog derivatives were designed, synthesized and allowed to evaluate for their anti- proliferative and apoptosis induction potential against cervical (HeLa), breast (MCF-7 and MDA-MB-231) and lung (A549) cancer cell lines relative to normal HEK293 cells. The MTT assay in conjunction with mitochondrial potential assays and the trypan blue dye exclusion were employed to ascertain the effects of the derivatives on the cancer cells. Further, mechanistic studies were conducted on compound **14a** to understand the biochemical mechanisms and functional interactions with various signaling pathways triggered in HeLa and MCF-7 cells. Compound **14a** induced apoptosis via caspase independent pathway through the participation of mitogen-activated protein kinases (MAPK) such as extracellular signal related kinase (ERK) and p38 as well as p53 pathways. It originates the activation of pro-apoptotic proteins such as Bak and Mcl-1s and also strongly induced the generation of reactive oxygen species. In downstream signaling pathway, activated p53 protein interacted with MAPK pathways, including SAPK/c-Jun N-terminal protein kinase (JNK), p38 and ERK kinases resulting in apoptotic cell death. The involvement of MAPK cascades such as p38, ERK and p38 on compound **14a** induced apoptotic cell death was evidenced by the fact that the inclusion of specific inhibitors of p38, ERK1/2 and JNK MAPK (SB2035809, PD98059 and SP600125) prevented the compound **14a** towards induced apoptosis. The results clearly showed that MAP

kinase cascades were crucial for apoptotic response in compound **14a** induced cellular killing and were dependent on p53 activity. Based on the results, compound **14a** was identified as a promising candidate for cancer therapeutics and these findings furnish a basis for further *in vivo* experiments on anti-proliferative activity.

Keywords: Bis(indole)hydrazide-hydrazone, anti-proliferative, apoptosis, MTT assay, mechanistic studies.

*Corresponding author Email: rrraju1@gmail.com

#Co- Corresponding author Email: cgkumar5@gmail.com

1. Introduction

Heterocyclic moieties play a vital role in the synthesis of potent drug molecules. Most of the heterocyclic systems with two or more hetero atoms act as anticancer agents in cancer chemotherapy and showed better anticancer results towards different human tumor cancer cell lines.[1-10] Indole moiety compounds are considered as most ubiquitous heterocyclic privileged scaffold and these compounds act as variety of potent therapeutic agents with different pharmacological activities such as antioxidant,[11] anti-HIV,[12,13] anticancer[14-19] and anti-rheumatoidal[20]. Indole moiety attached to different heterocyclic compounds containing various functional groups have lead to the enchanting array of potent bioactive natural products and also a variety of most active pharmaceutical ingredients.[21-24] Indolyl glyoxalyl amide (D-24851)[25] type indole built simple small molecules act as potent active anticancer targets and block the cell cycle transition predominantly at G_2/M phase followed by destabilization of microtubules.

Similarly, the pharmaceutical ingredient with -CO-NH-N=CH- (hydrazide-hydrazones) showed different biological activities including anti-tumor,[26-29] anti-malarial,[30] anti-convulsant,[31] anti-inflammatory,[32] antimicrobial,[33] antileishmanial,[34] anti-tubercular[35].

Further improvements lead to the synthesis of oxindole hydrazides with IC_{50} values ranging between 0.19-0.97 μM against potent inhibitors of tubulin polymerization.[36] 3-phenyl-5-sulfon-amidoindole-2-carboxylic acid hydrazide derivatives[37] were known to act as anti- depressant agents at 100 mg/kg dose. The hydrazide derivatives of 5-chloro-3-methyl-indole-2-carboxylic acid benzylidene[38] function as powerful apoptotic inducers against T47D

(breast cancer cell line), with IC_{50} value of 0.2 µM by obstructing tubulin polymerization in G2/M phase. 3,4,5-trimethoxy benzohydrazides[39] showed their antitumor activities against human prostate cancer cell line (PC3). Aryl hydrazone derivatives of 5-butyl-2-(4-methoxyphenyl)indole-3-carbaldehydes[40] showed potent growth inhibitory activity against breast cancer cell lines with IC_{50} values ranging between 19-115 nM followed by cell cycle arrest in G_2/M phase resulting in apoptosis.

A library of bis(indolyl)ketohydrazide-hydrazones were screened for their anticancer activities against HCT-116, MCF-7, JURKAT and MDA-MB-231 cancer cell lines. The most active compound, 4-chloro benzyl derivative showed caspase-dependent apoptosis in cells. This compound also arrested cell cycle in G2/M phase by restricting tubulin polymerization with IC_{50} value of 0.6 µM.[41] Bis(indolyl)hydrazide-hydrazone derivatives[42] were screened for their anti-cancer activity with IC_{50} values ranging between 1.0 to >100 µM against six human cancer cell lines. N'-((5-Methoxy-1*H*-indol-3-yl)methylene)-1*H*-indole-2-carbohydrazide[43] was efficient and most selective agent with a incredible ability to encourage apoptosis and mitotic block in A549 (lung adenocarcinoma) cell line by concentrating the cellular microtubule system through tubulin binding. Coscinamides A-C were extracted from marine sponge *Coscinoderma* sp. and having with a linear alpha-keto enamide spacer. Coscinamide B[44] exhibit anti-cancer activity against human prostate cancer cell line (IC_{50} = 7.6 µg/mL). The structures of potent anticancer compounds are shown in Figure 1.

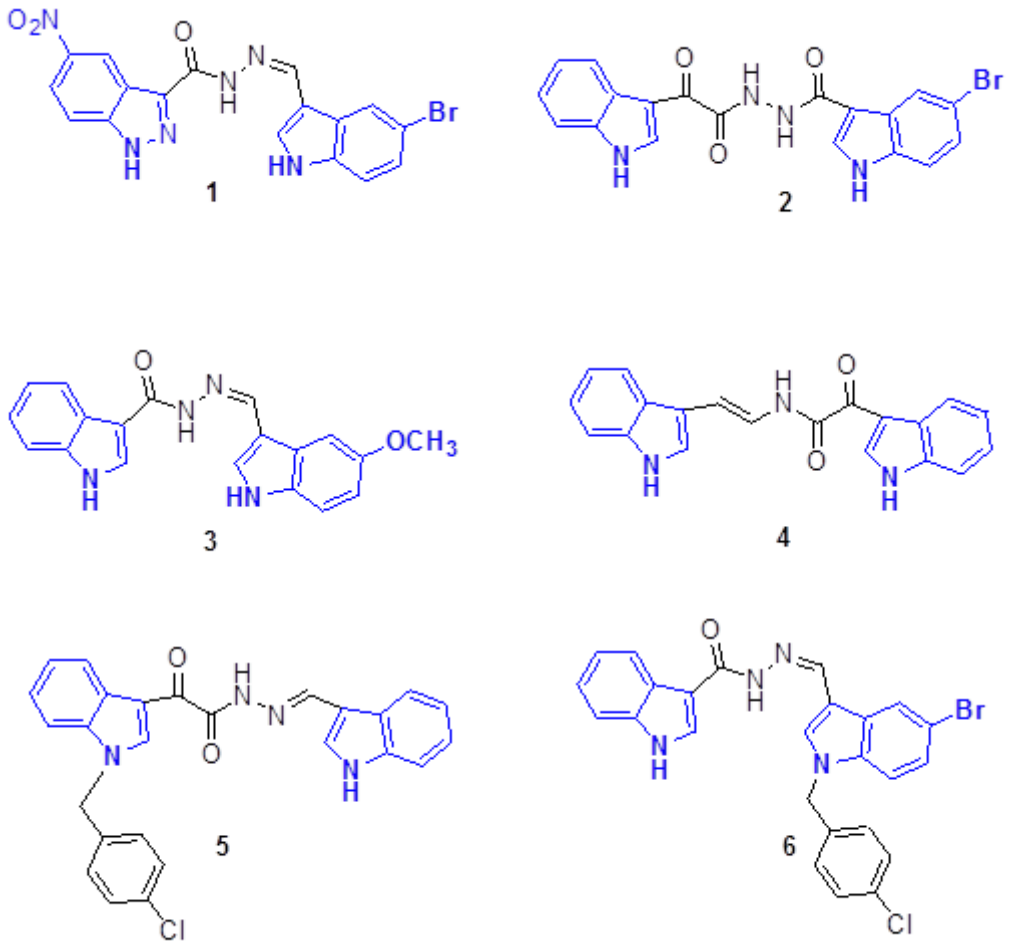

Figure 1: Structures of potent anticancer bisindole compounds.

Previously, a series of novel indole-indazolyl hydrazide-hydrazone derivatives were synthesized and screened for their anti-tumor activities against HeLa, A-549, MDA-MB-231, and MCF-7 cancer cell lines and showed IC_{50} values varied from 1.93 to 29.58 µM, respectively.[6] Further, bis(indolyl) triketo diazo compounds[45] were also synthesized and screened for anticancer activities against HeLa, A-549, MDA-MB-231, and MCF-7 human cancer cell lines which showed IC_{50} values varied from 1.3 to 44.5 µM, respectively. The remarkable significant activity of these indole-indazolyl hydrazide-hydrazones motivated us to synthesize N-methyl and N,N-dimethyl bis(indolyl)hydrazide-hydrazone derivatives. These compounds were subjected to cytotoxicity against cervical (HeLa), breast (MCF-7, MDA-MB-231) and lung

(A549) cancer cell lines. The cytotoxicity of these compounds were also checked against human embryonic kidney (HEK293) cells.

2. Results and discussion

2.1 Chemistry

Vilsmeir-Haack reaction of Indole and 5–bromo indoles **7a-b** with $POCl_3$ and DMF gave indole-3-carboxaldehydes **8a-b** in good yields.[46,47] These indole carboxaldehydes were converted to corresponding indole carboxylic acid derivatives **9a-b**[48] with $KMnO_4$ and acetone solvent. This acid derivatives were refluxed with conc. H_2SO_4 and methanol mixture over 6 to 7 hours period then gave the ester compounds **10a-b.**[49] N-methyl indolyl derivatives were obtained from ester compounds by refluxing with dimethyl carbonate and K_2CO_3 in DMF solvent over 4 hours time period.[50] Finally, Indolyl carbohydrazide derivatives (**12a-b**) were achieved by refluxing the N-protected ester with hydrazine hydrate and ethanol solvent over 8 – 10 hours time period (**12a-b**) in good yields.

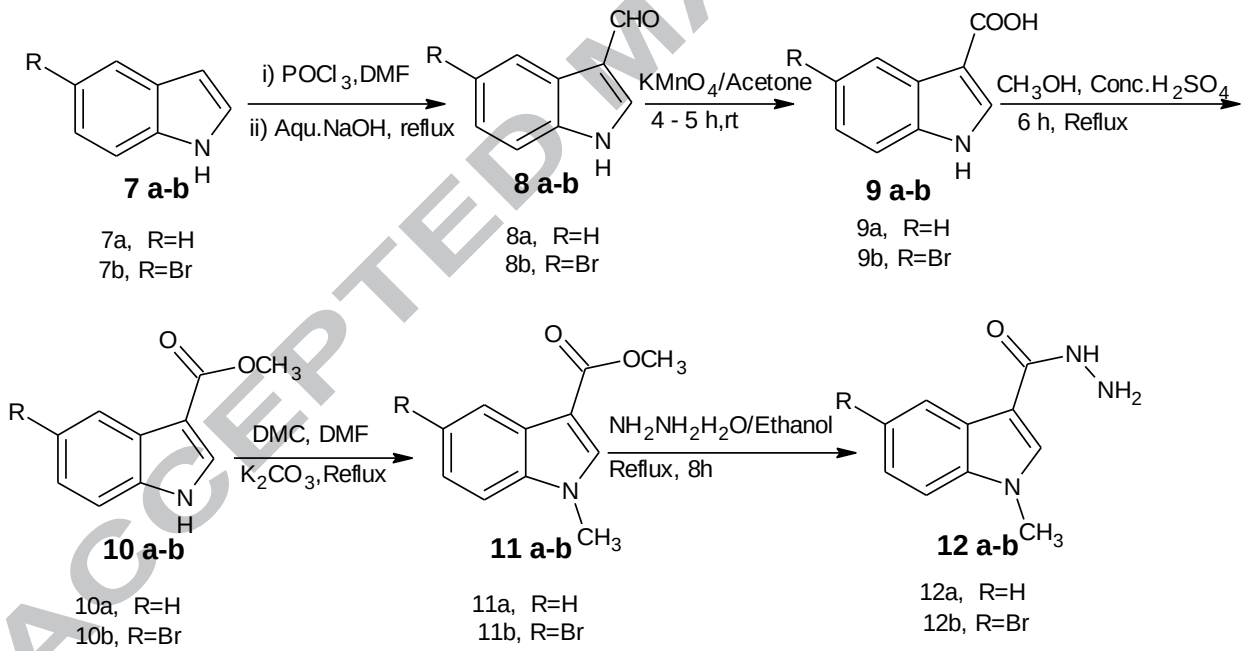

Scheme 1: Synthesis of N-methyl indole-3-carbohydrazide derivatives

Finally, the reaction of N-methyl indolyl -3-carbohydrazides **12a-b** with different indole-3-carboxaldehydes **13a-13c** in the presence of glac. CH_3COOH at 90^oC over a period of 6 h to afford N-methyl and N,N-dimethyl bis(indolyl) hydrazide-hydrazones (**14a-14d**) in good yields.

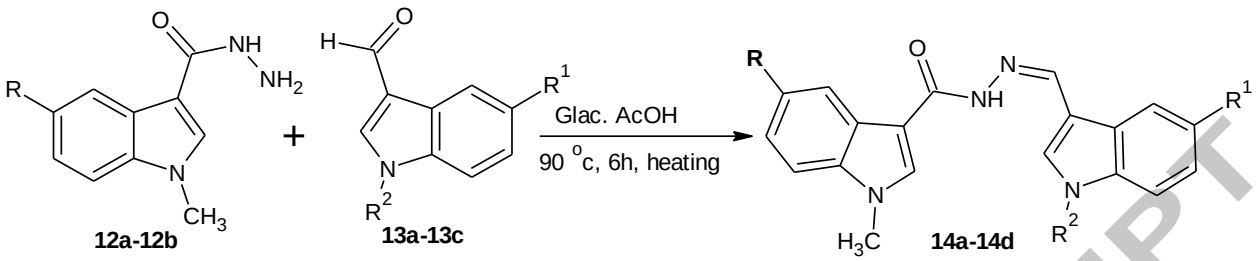

Scheme 2: Synthesis of bis(indolyl) hydrazide-hydrazone derivatives

Where, 12a, R=H
12b, R=Br

Where, 13a, R^1=H and R^2=CH_3
13b, R^1=H and R^2=H
13c, R^1=OCH_3 and R^2=H

Where, 14a, R=Br, R^1=H and R^2=CH_3
14b, R=H, R^1=H and R^2=CH_3
14c, R=Br, R^1=H and R^2=H
14d, R=Br, R^1=OCH_3 and R^2=H

2.2 Biological Evaluation

2.2.1 *In vitro* anticancer activity

Four compounds were screened for cytotoxicity against four different human cancer cell lines Such as Cervical cancer cell lines **(HeLa),** human breast adenocarcinoma cells **(MDA-MB-231 & MCF-7),** Human alveolar adenocarcinoma cells **(A549)** and normal human embryonic kidney cells **(HEK-293)** and shown in table 1. IC_{50} value is defined as the concentration at which 50% of cell lines shall be destroyed and represented in µM. The obtained values varied from 0.793-31.26 µM.

Compound **14a** was found to be the most potent analog especially on A549 with IC_{50} value of 0.793 µM and it may be identified as drug target in cancer chemotherapy. The removing of N-methyl from the compound **14a** gave **14c** which showed selective activity on MDA-MB-231 (IC_{50} = 14.25 µM). Compound **14b** exhibit moderate cytotoxicity on MDA-MB-231 (IC_{50} = 18.91 µM) and lung cancer cell lines A549 (IC_{50} = 18.96 µM). While the compound **14d** exhibited moderate cytotoxicity against HeLa and A549 with IC_{50} values of 14.25 µM and 12.85

μM respectively. The test compound **14a** showed potent selective cytotoxicity against A549 with IC_{50} = 0.793 μM, then it is selected for complete further mechanic studies.

Table 1: Cytotoxicity of synthesized derivatives **14a-14d**

Test compound	**IC_{50} (μM)**				
	HeLa	**MDA-MB-231**	**MCF-7**	**A549**	**HEK293**
14(a)	–	–	–	0.793 ± 0.29	-
14(b)	–	18.91 ± 0.57	31.26 ± 0.89	18.96 ± 0.72	-
14(c)	-	14.25 ± 0.41	-	-	-
14(d)	14.25 ± 0.45	22.74 ± 0.28	-	12.85 ± 0.39	-
Doxorubicin	0.36 ± 0.14	0.47 ± 0.4	0.98 ± 0.14	0.89 ± 0.26	-

"-" shows no activity.

2.2.2 Evaluation of *in vitro* anticancer activity of compound 14a on different cancer cell lines

The anticancer activity of compound **14a** on different cancer cell lines is shown in Table 1. The sensitive cancer cell lines to the test compound were MCF-7 (breast), HeLa (cervical) and SW-680 (colon) with IC_{50} values nearer to standard drug, "doxorubicin". In addition, MDA-MB-231 (breast cancer) and A549 (lung cancer) also showed high sensitivity to the test compound. The test compound also showed considerable anticancer activity towards head and neck squamous cell carcinomas (FaDu, SCC-25 and Detroit-562). As shown in Figure 2, compound **14a** exerted dose-dependent inhibition in all tested human tumor cell lines. It is noteworthy to mention that against HeLa, MCF-7 and SW-680 cell lines, maximum inhibitory activity was achieved. However, on MDA-MB-231 and A549 cell lines significant decline in cell growth was observed. In case of HNSCC (head and neck squamous cell carcinoma) cell lines such as FaDu and SCC-25 cell lines, the test compound showed considerable inhibitory activity and cell viability was reduced in a dose-dependent manner. It is noteworthy to mention that in normal HEK-293 cell line at higher concentration of 200 μM, 95% of total cells were viable indicating the non-toxic

nature of this compound on the normal cell line. On comparison of inhibition data, it was clearly established that a considerable reduction in cell viability was appeared in HeLa, MCF-7, SW-680, MDA-MB-231, A549 and the entire set of HSNCC cells; however, it was more significant against HeLa, MCF-7 and SW-680 cell lines. Since the test compound **14a** showed potent selective cytotoxicity against HeLa and MCF-7 with IC_{50} values of 1.69 and 1.19 μM, it was selected for further mechanistic studies.

Table 2. Cytotoxicity of compound **14a** against different cancer cell lines

Cell line	**IC_{50} values (in μM)**	
	Compound 14a	**Doxorubicin**
HeLa	1.69 ± 0.05	1.09 ± 0.11
MDA-MB-231	5.49 ± 0.35	3.1 ± 0.59
MCF-7	1.19 ± 0.07	0.23 ± 0.01
SW-680	2.77 ± 0.74	1.2 ± 0.9
A549	5.49 ± 0.35	2.11 ± 0.09
FaDu	9.64 ± 0.09	0.68 ± 0.14
SCC-25	10.13 ± 0.23	2.24 ± 0.11
Detroit-562	22.69 ± 1.44	1.26 ± 0.09
HEK-293 (Normal)	>200	>200

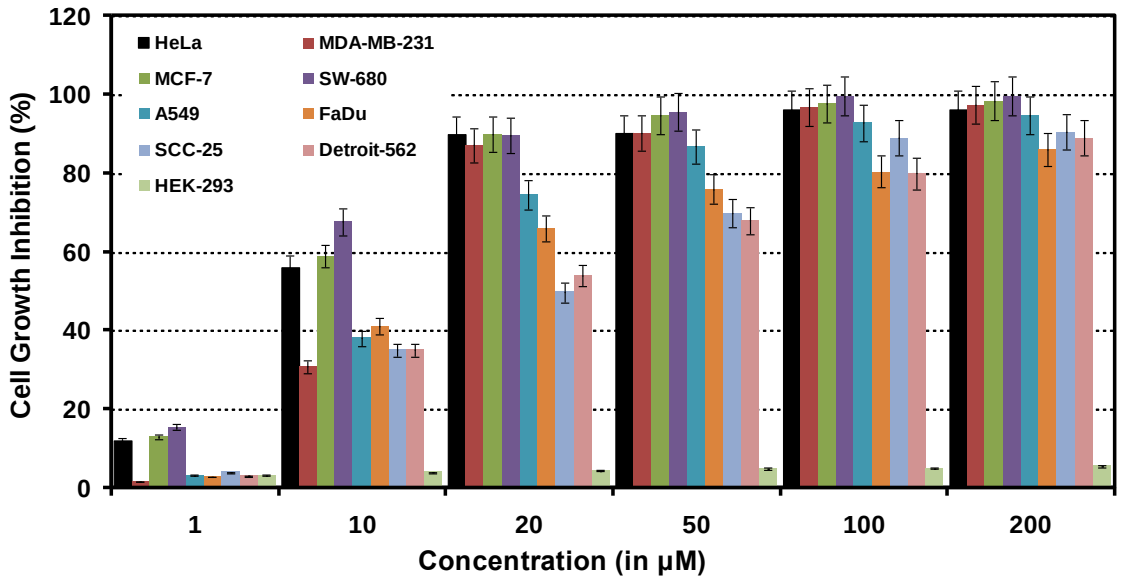

Figure 2: Dose dependent cell growth inhibition (%) of compound **14a** on different cancer cell lines

2.2.3 Annexin V/PI staining for cell apoptosis

Annexin V/propidium iodide (PI) co-staining assay was performed to decide the way of cell death encouraged by compound **14a.** This assay distinguish between necrotic cell death and apoptotic. HeLa and MCF-7 cell lines were reacted with compound **14a** (1 µM) for 8, 12 and 16 h, then double stained with FITC-conjugated annexin V and propidium iodide (PI), and it was analyzed by flow cytometry (Figure 3). After the completion of 12 h reaction with compound **14a**, a little amount of cell lines (~9%) had either inhibited or were in late stage of the apoptosis (Annexin V positive, PI positive), and ~24% of cancer cells were appeared in early stage of the apoptosis (Annexin V positive, PI negative). After 16 h of treatment to compound **14a**, ~76% of cells were appeared at the stage of dead/late apoptotic quadrant, ~26% of cells were appeared in the early stage apoptosis, and the final ~8% of the cell lines were viable. The experimental results were the average of three independent experiments treated with compound 14a incubated at time intervals of 8h, 12h and 16h. At 12 h of incubation, the data 9% refers to the percentage of cells that are Positive for both Annexin V and Propidium Iodide and 24% of cells were Annexin V positive and Propidium iodide negative suggesting the early stage of the apoptosis. After 16h of incubation the percentage of cells in late apoptosis were 76% suggesting that the cell death induced by compound 14a is due to apoptosis and not by necrosis. Thus, a remarkable quantity of cell lines progress with the Annexin V

positive/PI-negative quadrant, mightily suggesting that the observed anticancer activity in MCF-7 and HeLa cells is through apoptosis

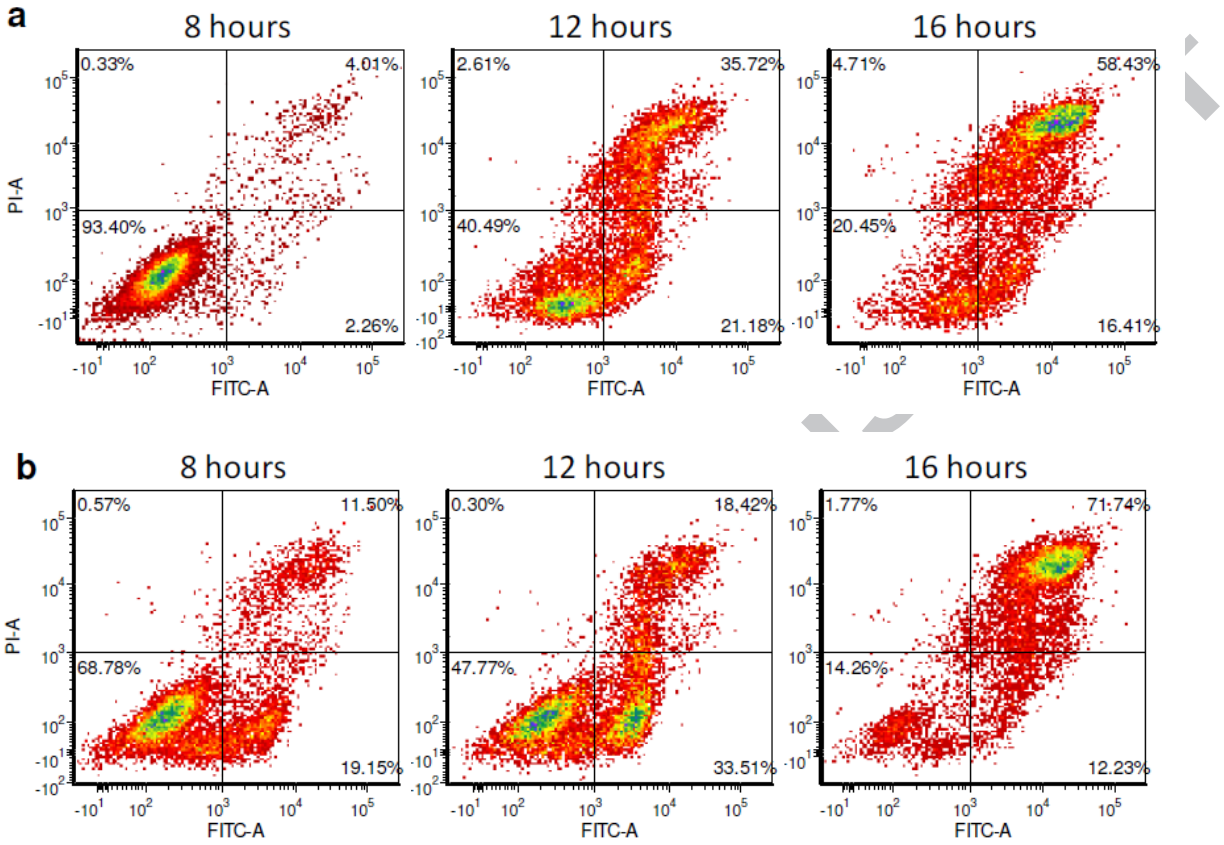

Figure 3: Effect of compound **14a** treatment for 8 to 16 h induced apoptotic cell death in (a) MCF-7 and (b) HeLa cancer cell lines evaluated based on Annexin V apoptosis assay

2.2.4 Cell cycle analysis

Treatment of HeLa and MCF-7 cells with compound **14a** caused no important changes in the levels of cell lines at each phase of the cell cycle over 16 hours time period (Figure 4). The data showed that compound **14a** did not produce cell cycle arrest in these cancer cell lines. The inability of compound **14a** to induce cell cycle arrest suggests that topoisomerase obstruction can not be the first mechanism of action for compound **14a**, since small molecules functioning as topoisomerase inhibitors were known to arrest the cells in definite phases of cell cycle.

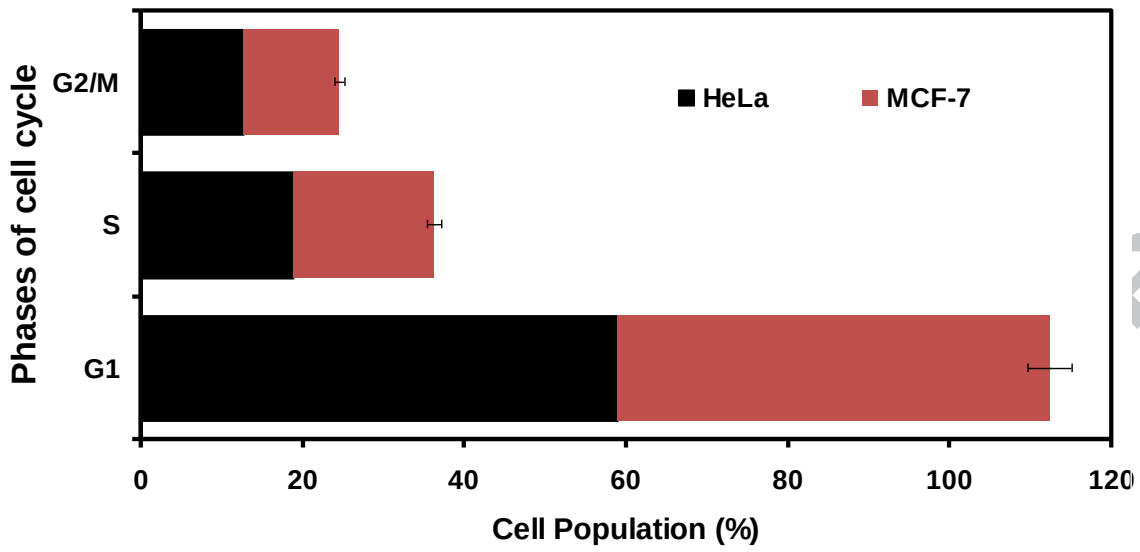

Figure 4. Effect of compound **14a** on cell cycle arrest. MCF-7 and HeLa cell lines were exposed to compound **14a** (1 μM) for 16 h. Values are represented as the percentage of the cell population in G1, S and G1/M phases of cell cycle. $P<0.05$, significantly different from the vehicle group.

2.2.5 ROS production

To determine if ROS production is induced in response to compound **14a** treatment and it is achieved the cause of demise of reacted cancer cell lines, MCF-7 and HeLa cells were reacted with **14a** and produced ROS levels were observed with DCF(dichlorofluorescein diacetate), which is a non-fluorescent dye that treated with peroxides to afford fluorescent dichlorofluorescein. Flow cytometry was used to quantify the dye in live cells with the level of intracellular fluorescence. t-butyl peroxide was used as positive control for these experiments and it create the peroxides in cancer cells. As compared to t-BHP, cells treated with compound **14a** at 5 μM concentration produced significant amount of ROS in 4 h, as indicated by DCF staining (Figure 5) in both HeLa cells (29.9%) and MCF-7 (36.8%). After 8 h of incubation, ROS production in both HeLa and MCF-7 cells increased to 58.9% and 48.27%, respectively. However, when compound **14a** treated cells were pretreated with NAC, a known ROS inhibitor; a significant reduction in the ROS production in both HeLa and MCF-7 cells was observed. This clearly indicates that there is a rapid formation of ROS upon compound **14a** treatment which

suggests that it directly produced by compound **14a** treatment and its not a byproduct of cell death.

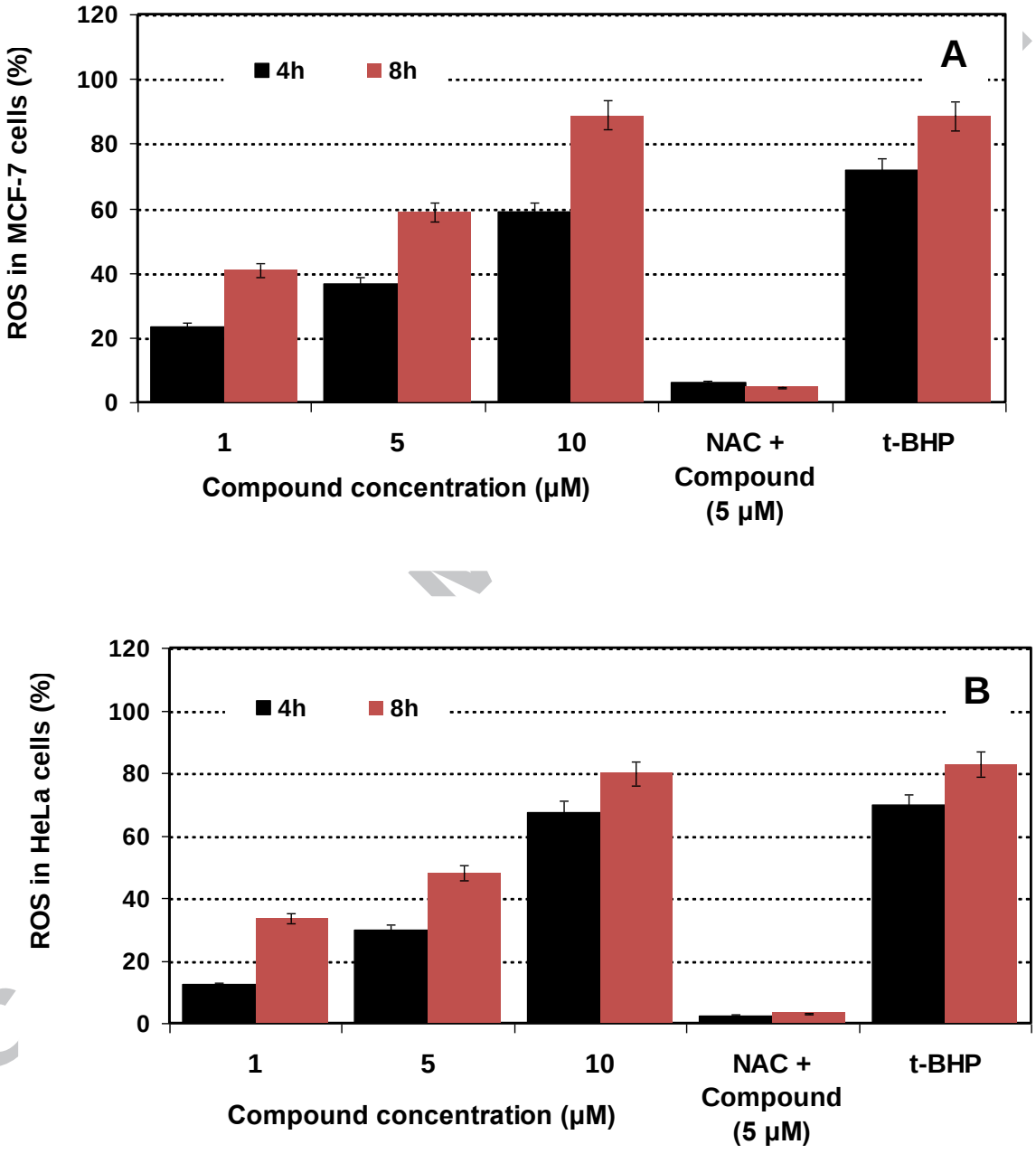

Figure 5. Effect of compound **14a** on ROS production. (A) MCF-7 and (B) HeLa cell lines when exposed to compound **14a** (1 µM) for 3 h. ROS production was monitored using DCFH-DA assay. $P<0.05$, significantly different from the vehicle group.

2.2.6 NO production

The experimental analysis showed that in both HeLa and MCF-7 cancer cells, the compound **14a** induced NO production in a dose-dependent way. Through the primary drug target interactions, compound **14a** at 5 μM produced significant levels of NO production after 8 h of treatment, as indicated by Griess reagent analysis (Figure 6). In case of MCF-7 cells, the NO levels produced by treatment with compound **14a** at concentrations 1 and 5 μM were 32.1% and 48.9%, respectively. Similar effect was found in HeLa cells where the observed NO levels were 29.8% and 42.4% at 1 and 5 μM, respectively. The results demonstrated that through primary drug target interactions, compound **14a** caused oxidative stress response in both HeLa and MCF-7 cells, thereby induced production of NO, a secondary messenger molecule which is responsible for the downstream signaling process leading to apoptotic cell death.

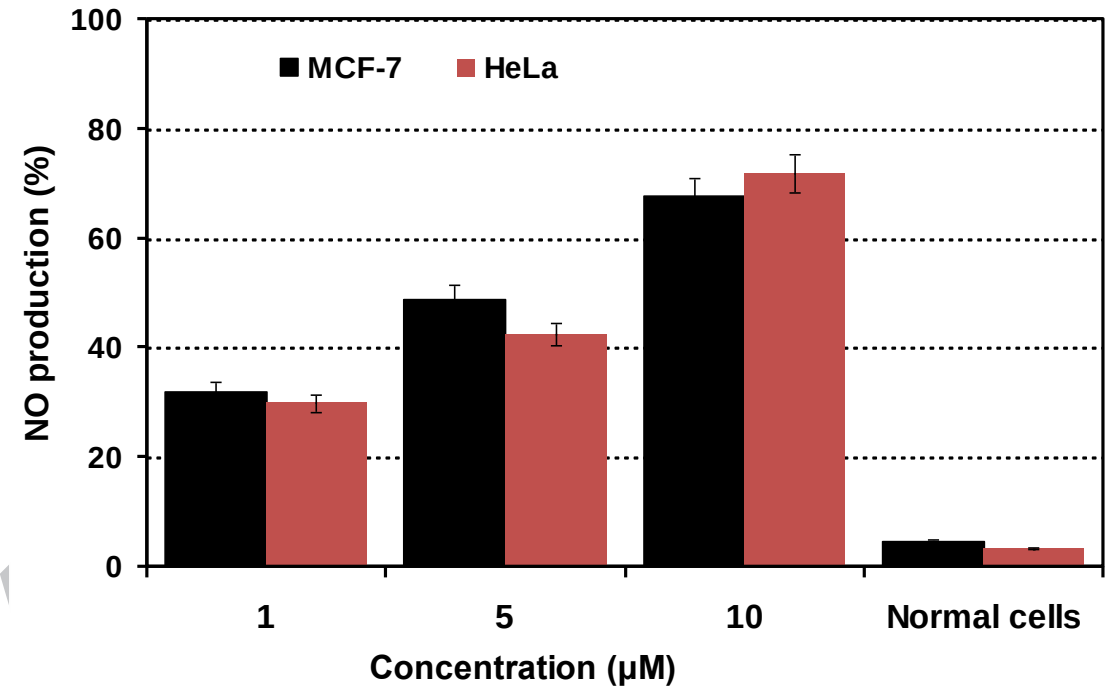

Figure 6: Effect of compound **14a** on NO production. MCF-7 and HeLa cells were exposed to compound **14a** at concentrations of 1, 5 and 10 μM for 8 h. NO production was monitored using Griess reagent assay. $P<0.05$, significantly different from the vehicle group.

2.2.7 Effect on PKA, ABL, and PTP1B enzymes

The enzymes used in the study such as tyrosine kinase ABL (ABL), cAMP-dependent protein kinase A (PKA) and protein-tyrosine phosphatase 1B (PTP1B) plays a key role in anticancer drug discovery. PTP1B is a positive factor in cancer phenotypes; PKA and ABL are the protein kinases where the proteins are mostly mutated in malignant tumors.

Compound **14a** moderately inhibited the activity of PKA and ABL and exerted moderate effect on the phosphorylation of these twice protein kinases (Figure 7). However, a dose-dependent inhibitory effect of PKA activity was appeared. At a concentration of 50 µM, compound **14a** inhibited 45% of the measured PKA activity. Similarly, compound **14a** was found to restrict PTP1B in a dose-dependent way (Figure 7). The PTP1B activity was inhibited by 48% at 50 µM concentration of compound **14a**. The results demonstrated that compound **14a** is a cytotoxic compound, which exibit its anti-proliferative effects through various mechanisms that add the generation of oxidative species such as ROS and NO and inhibition of protein kinase activity.

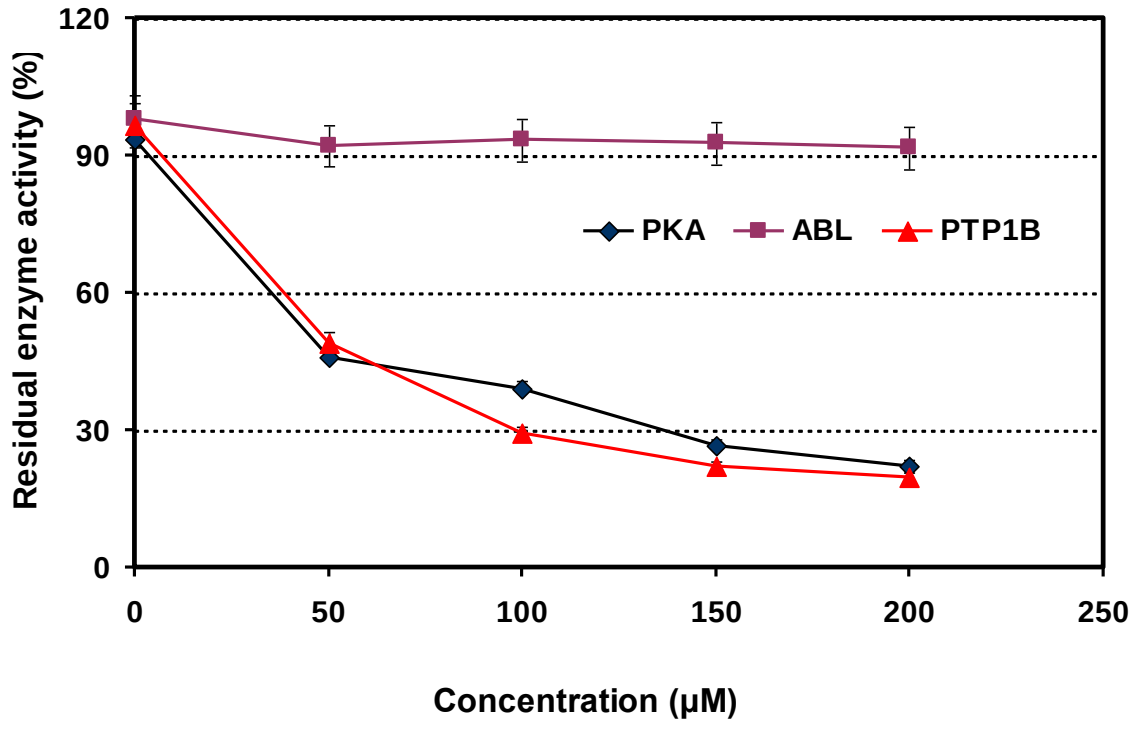

Figure 7: The effect of compound **14a** on the enzymatic activity of cAMP-dependent protein kinase A (PKA), protein-tyrosine phosphatase 1B (PTP1B) and tyrosine kinase ABL (ABL). Enzyme activity was monitored in two separate experiments and results are noted as % of control activity in the absence of compound **14a**. Each point represents the average of two parallel run means.

2.2.8 Mitochondrial membrane potential in HeLa and MCF-7 cell lines

The mechanism of action of anticancer activity of compound **14a** on HeLa and MCF-7 cell lines was studied by evaluating caspase dependent and caspase independent apoptotic pathways. Mitochondria plays an important characteristic role in both extrinsic and intrinsic apoptosis pathways and hence the effect of compound **14a** on mitochondrial membrane potential was measured. Compound **14a** affected the mitochondrial membrane potential and related proteins. HeLa and MCF-7 cell lines were exposed to compound **14a** at a concentration range of 5 µM for the mentioned times (1 h, 2 h, 4 h and 8 h) and were analyzed by flow cytometry (Figures 8A and 8B). Results showed a band shift situation observed after incubation over 1 h and 2 h in both HeLa and MCF-7 cells, respectively; these phenomena were changed significantly over 4 h time period. These results indicate that compound **14a** affected the mitochondrial membrane potential.

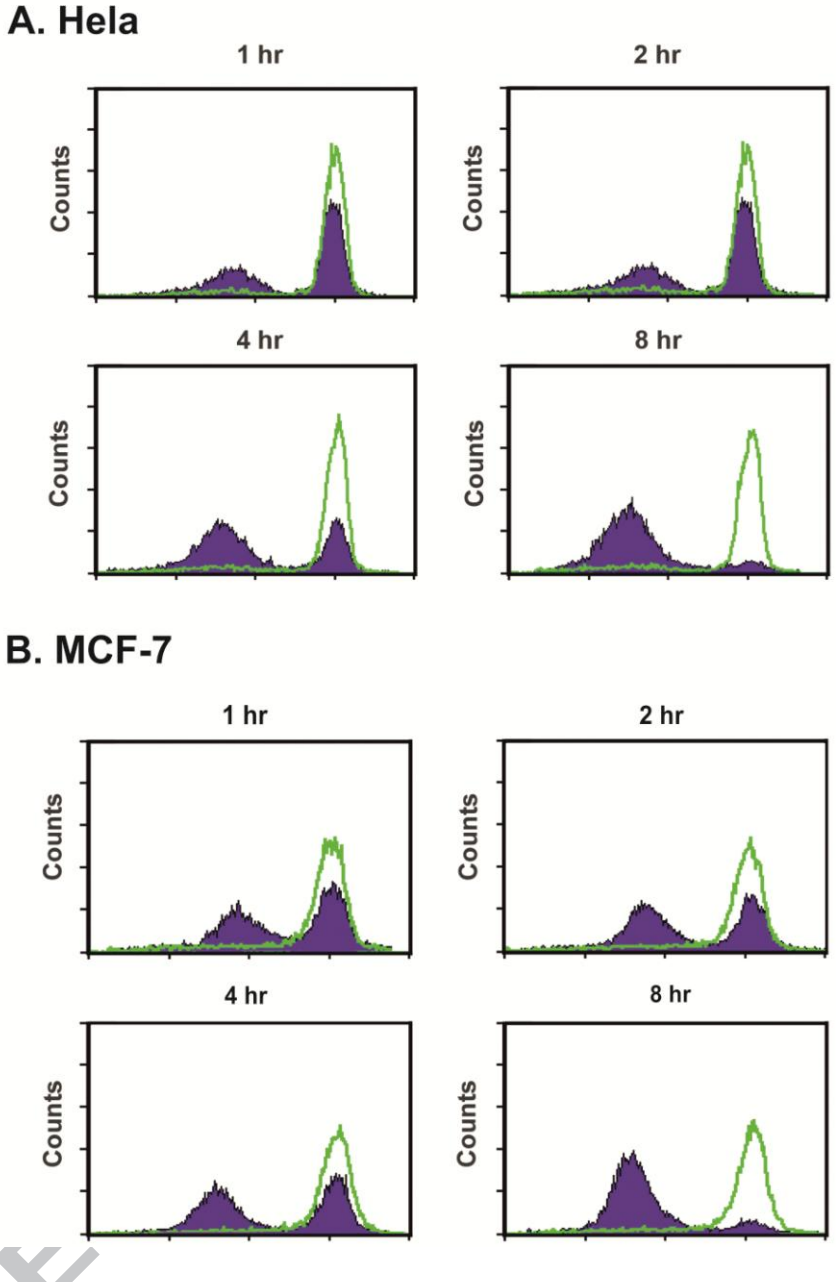

Figure 8: Effect of compound **14a** on the mitochondrial membrane potential in (**A**) HeLa and (**B**) MCF-7 cell lines. The cells were treated with 10 µM rhodamine 123 and incubated at 37 °C for 30 min in the presence of 5 µM of compound **14a** and then quantified by flow cytometric analysis at 1 h, 2 h, 4 h and 8 h with rhodamine 123. The horizontal axis shows the relative fluorescence intensity, and the vertical axis indicates the cell counts or cell number. The green curve indicates the control. The blue curve indicates **14a** treated cells. Loss of mitochondrial membrane potential denotes the shifting from green curve to the blue curve. Data are expressed from at least three separate determinations.

2.2.9 Caspase activation in HeLa and MCF-7 cells

In both extrinsic and intrinsic apoptotic pathways, the activation of caspase pathway engage an important role. The activation of caspases – 3 play a crucial role among the caspases in the induction of apoptotic cell death occurred in apoptosis pathway. Hence, the role of compound **14a** in the activation of caspase-3 was studied in both MCF-7 and HeLa cell lines. The results demonstrated that in both MCF-7 and HeLa cell lines, caspase-3 was not activated by compound **14a** (Figures 9 and 10). In addition, the positive control - paclitaxel (3 µM) activated caspase-3 in both HeLa and MCF-7 cell lines.

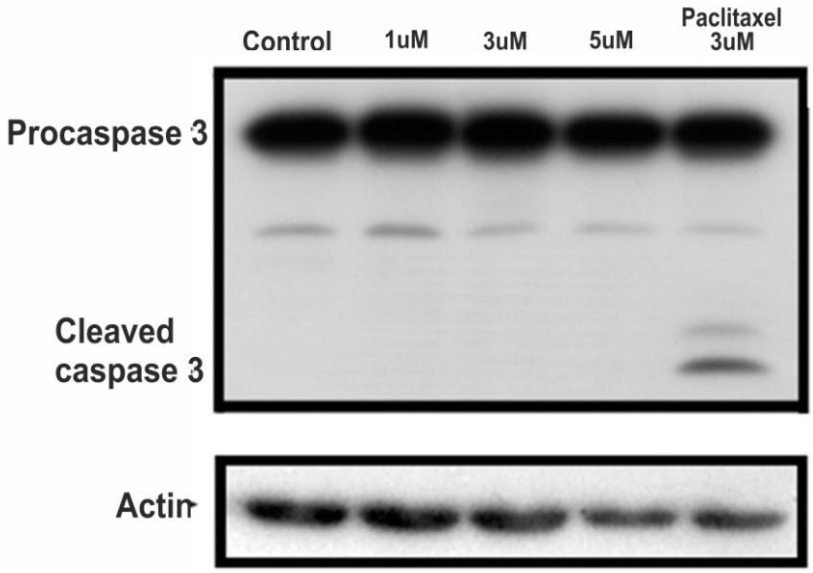

Figure 9: Effect of compound **14a** on caspase-3 activation in HeLa cell line. HeLa cells were treated with compound **14a** at concentrations 1, 3 and 5 µM for 24 h and caspase-3 activation was detected using Western blot analysis. Paclitaxel at 3 µM was used as a positive control.

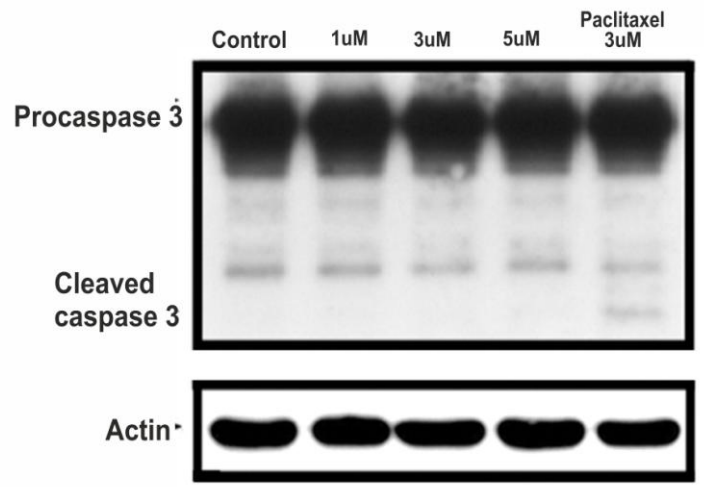

Figure 10: Effect of compound **14a** on caspase-3 activation in MCF-7 cell lines. MCF-7 cells were treated with compound **14a** at concentrations 1, 3 and 5 µM for 24 h and caspase-3 activation was detected using Western blot analysis. Paclitaxel at 3 µM was used as a positive control.

In addition to caspase-3, the activation and cleavage of caspase -6, -7, -8, and -9 was not observed upon the treatment with **14a** in both MCF-7 and HeLa cell lines, even at 5 µM concentration for 24 h (Figure 11 and 12). The results demonstrate that compound **14a** induced apoptotic cell death in both MCF-7 and HeLa cell lines which is independent of caspase activation.

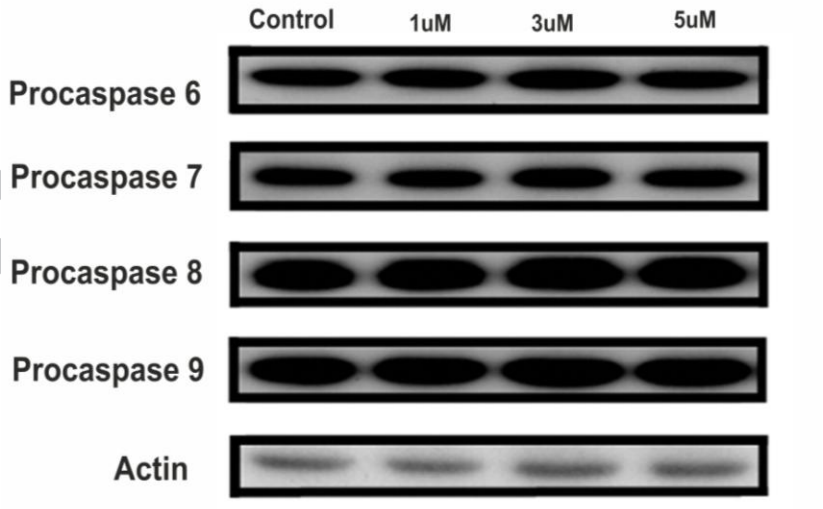

Figure 11. Effect of compound **14a** on caspase-6, 7, 8 and 9 activation in HeLa cell lines. HeLa cells were treated with compound **14a** at concentrations 1, 3 and 5 µM for 24 h. The proteins were separated and activation of caspase-6, 7, 8 and 9 were evaluated using Western blot analysis.

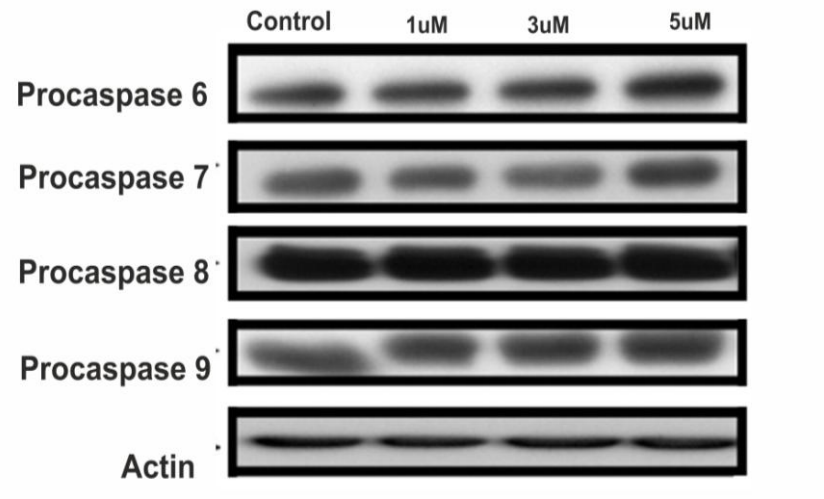

Figure 12. Effect of compound **14a** on caspase-6, 7, 8 and 9 activation in MCF-7 cell line. MCF-7 cells were treated with compound **14a** at concentrations 1, 3 and 5 μM for 24 h. The proteins were separated and activation of caspase-6, 7, 8 and 9 were evaluated using Western blot analysis

2.2.10 Expression of pro-apoptotic and anti-apoptotic proteins in HeLa and MCF-7 cells

The effect of compound **14a** on Bcl-2 family protein expression which was known to play an important crucial role in the mitochondria, including the study of mitochondrial membrane potential mediation. The results demonstrated that in both HeLa and MCF-7 cells, compound **14a** showed no effect on the regulation of Mcl-1 long form (Mcl-1L) protein, which moderate inhibition of cell apoptosis (anti-apoptotic). However, compound **14a** induced the expression of the Mcl-1 short form (Mcl-1s) protein (pro-apoptotic), which encourages the apoptotic cell death (Figure 13 and 14).

Furthermore, in both MCF-7 and HeLa cell lines, there was no change in the expression levels of Bcl-2 and Bid proteins (Figure 13 and 14). The results demonstrated that in both HeLa and MCF-7 cells, Bak and Mcl-1 played an crucial role in compound **14a** induced caspase independent apoptotic cell death.

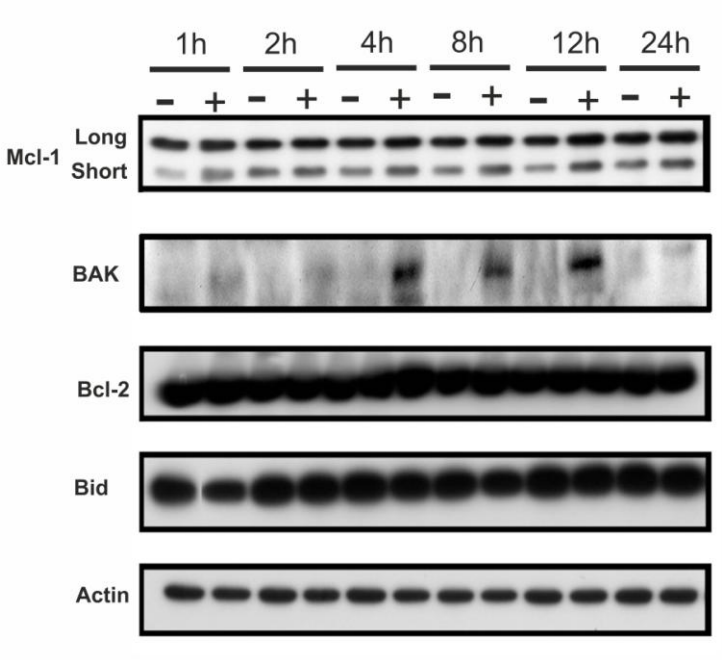

Figure 13: Effect of compound **14a** on mitochondrial apoptotic or anti-apoptotic protein levels in HeLa cells. In HeLa cells, compound **14a** induced upregulation of Mcl-1s and Bak (pro-apoptotic) proteins whereas Bcl-2 and Bid protein levels were not affected by compound **14a** treatment. Cells were treated with 5 μM of compound **14a** for 24 h and proteins were detected by Western blotting. Data are expressed from at least three separate determinations.

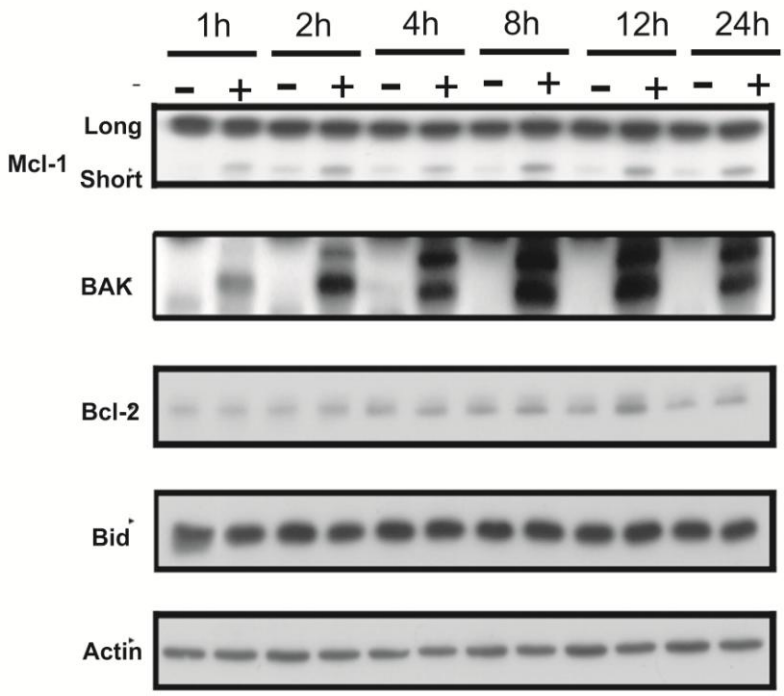

Figure 14: Effect of compound **14a** on mitochondrial apoptotic or anti-apoptotic protein levels in MCF-7 cells. In MCF-7 cells, compound **14a** significantly induced the activation of Bak and also upregulated Mcl-1s expression. On the other hand, Bcl-2 and Bid protein expressions remained unchanged upon treatment with compound **14a**. Cells were treated with 5 µM of compound **14a** for 24 h and proteins were detected by Western blotting. Data are expressed from at least three separate determinations.

2.2.11 Oxidative stress induction

Reactive oxygen species is an important biomarker of apoptosis. The increase in intracellular ROS eventually induces apoptosis and cell cycle arrest. In this study, the effect of compound **14a** on ROS induction at 12 h and 24 h in MCF-7 and HeLa cells was evaluated using H2DCFDA dye and the histograms are shown in Figures 15 and 16. It is clearly evident that in cells treated with compound **14a** (blackpanel), ROS concentration increased in a time dependent way as compared to the untreated control (pink panel). From the histograms, it was observed that in case of HeLa cells treated with compound **14a**, ROS were induced at 12 h as compared to untreated cells (Figure 15). However, in case of compound **14a** treated MCF-7 cells, ROS induction was pronounced at 24 h as compared to untreated cells (Figure 16).

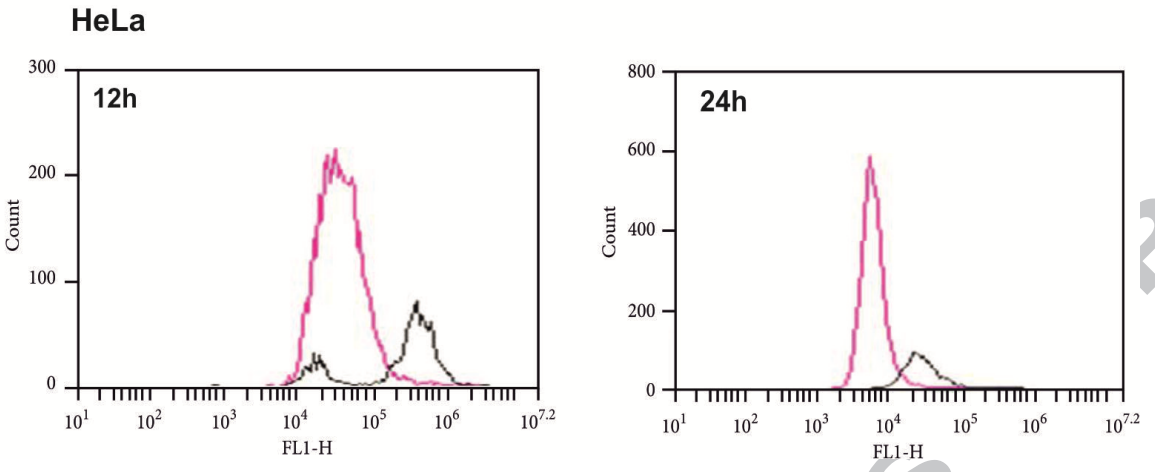

Figure 15: Representative histograms of treated and untreated HeLa cells stained with CM-H2DCFDA dye. The pink histogram depicts stained untreated control cells while black shows the cells treated with 5 µM of compound **14a** at 12 and 24 h, respectively.

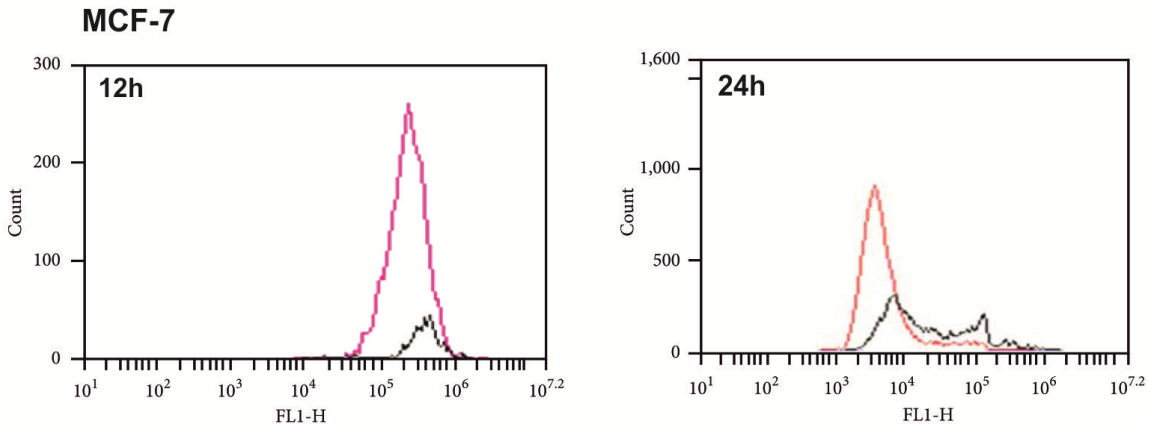

Figure 16: Representative histograms of treated and untreated MCF-7 cells stained with CM-H2DCFDA dye. The pink histogram depicts stained untreated control cells while black shows the cells treated with 5 µM of **14a** at 12 and 24 h, respectively.

2.2.12 Acetylation of p53

The effect of compound **14a** on the induction and acetylation status of p53 levels in both MCF-7 and HeLa cell lines during cell apoptosis was investigated using ELISA assay. The results are expressed as control index and are shown in Figure 17. From the results it is clearly evident that, compound **14a** could induce p53 acetylation in MCF-7 and HeLa cells and also significant increase in total p53 protein levels were observed in a time-dependent way. After 24 h of the reaction with compound **14a** in HeLa cells (Figure 17), the acetylated p53 levels were upregulated as compared to control cells (DMSO treated). Similar increase in acetylated p53 levels was observed in MCF-7 cells after 24 h of treatment (Figure 18). In case of total p53 levels, a significant upsurge in both HeLa and MCF-7 cancer cell lines was observed with increasing time i.e., after 12 h of treatment. In control untreated cells, a negligible effect was observed on total p53 levels in both cell lines at time intervals studied (Figure17 and 18).

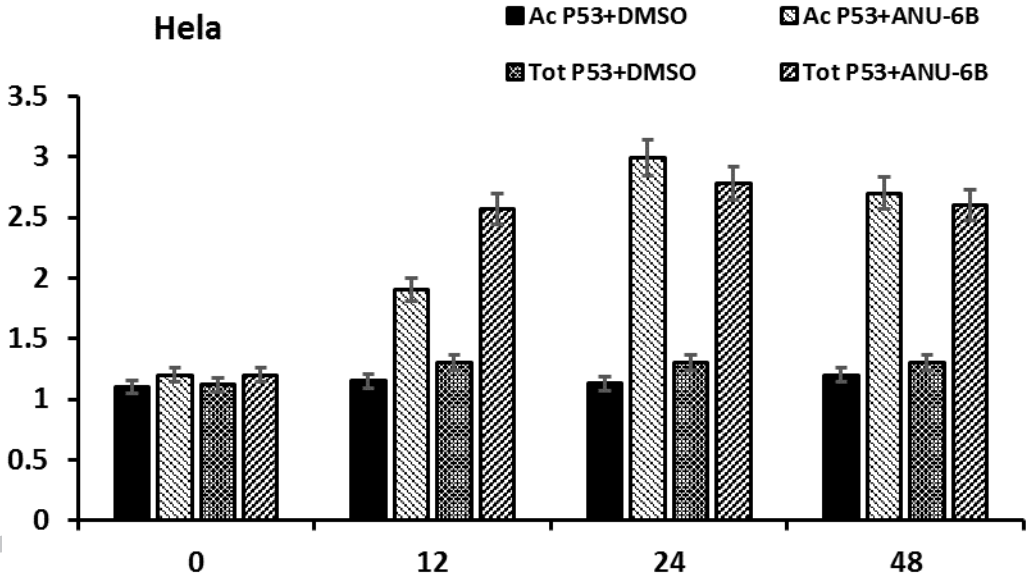

Figure 17: The ELISA assay of total and acetylated p53 protein levels expressed in Hela cells based on control index. Cells were treated 5 µM of compound **14a** for 0, 12, 24 and 48 h. Values are the means ± SD of triplicate experiments. **P*<0.001 vs. all other groups in different times. Total P53 in HeLa cells without compound **14a** treatment and with compound **14a** treatment at time periods 12, 24 and 48 h. No significant difference was shown in total and acetylated p53 content in other groups.

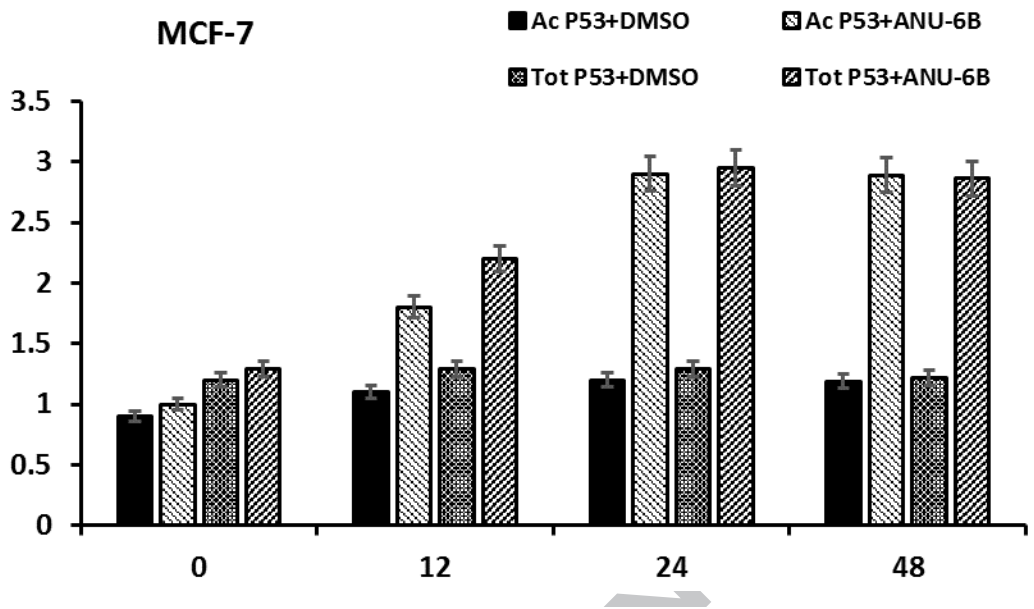

Figure 18: The ELISA assay of total and acetylated p53 protein levels expressed in MCF-7 cells based on control index. Cells were treated 5μM of compound **14a** for 0, 12, 24 and 48 h. Values are the means ± SD of triplicate experiments. **P*<0.001 vs. all other groups in different times. Total P53 in HeLa cells without compound **14a** treatment and with compound **14a** treatment at time periods 12, 24 and 48 h. No significant difference was shown in total and acetylated p53 content in other groups.

2.2.13 Activation of MAPK in HeLa and MCF-7 cells

The role of MAPK activation in compound **14a** induced MCF-7 and HeLa cells was elucidated *in vitro* through the protein phosphorylation assessment. Compared with positive control, 5 μM IC_{50} value of the compound **14a** efficiently induced through the activation of MAPK in cervical (HeLa) cell lines (Figure 19) and indicated with enhanced p-P38/total P38 (P=0.0168; Figure 19A), p-ERK1/2/total ERK1/2 (P=0.0002; Figure 19B), and p-JNK/total JNK ratio (P=0.0034; Figure 19C). However, MAPK activation was totally restricted by pre-treatment with the P38 kinase inhibitor SB2035809 (P=0.0187; Figure 19A), ERK1/2 inhibitor PD98059 (P=0.0003; Figure 19B) and JNK inhibitor SP600125 (P=0.0022; Figure 19C). Similarly, MCF-7 cells upon exposure to compound **14a** (5 μM) significantly induced MAPK activation (Figure 20), as evidenced by enhanced levels of p-P38/total P38 (P=0.0075; Figure 20A), p-ERK1/2/total ERK1/2 (P<0.0001; Figure 20B), and p-JNK/total JNK ratio (P=0.0022; Figure 20C).

Furthermore, this MAPK activation was significantly attenuated by pretreatment with the P38 kinase inhibitor SB2035809 (P=0.0187; Figure 20A), ERK1/2 inhibitor PD98059 (P=0.0003; Figure 20B) and JNK inhibitor SP600125 (P=0.0019; Figure 20C). MAPK is required for maintenance of the malignant state, but that short-term activation of MAPK may direct cells to apoptosis. Phosphorylation of p53 determines the biological activity of the protein. At several serine residues, including serine 6 and serine 15, phosphorylation has been shown to be relevant to DNA damage and apoptosis. Compound 14a showed activation and nuclear translocation of MAPK (extracellular signal-regulated kinase 1/2) and cellular abundance of the oncogene suppressor protein p53, phosphorylation of p53, and abundance of c-*fos*, c-*jun*, and *p21*. Thus, compound 14a acts via a ERK1/2-MAPK kinase-MAPK signal transduction pathway to increase p53 expression, phosphorylation of p53, and p53-dependent apoptosis in MCF-7 and Hela cell lines.

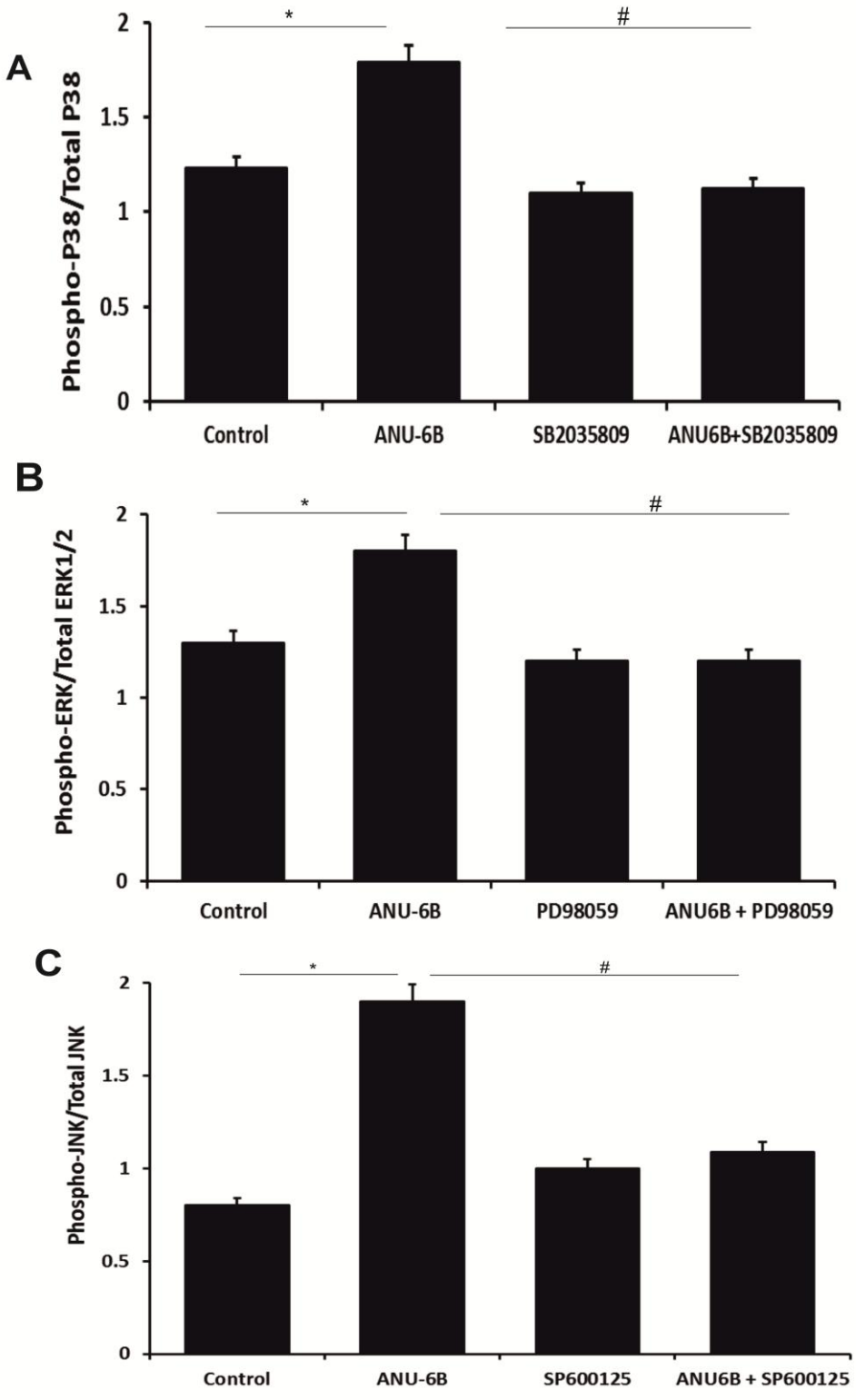

Figure 19: Effect of compound **14a** on activation of MAPK pathway in HeLa cells. **(A)** Phosphorylation of P38, **(B)** ERK1/2, and **(C)** JNK was determined by cell-based ELISA and expressed as the ratio of the phosphorylated to the total form of each protein. n=3 and **P*<0.0001 vs. control and $^{\#}P$<0.0001 vs. compound **14a** in the presence of SB2035809, PD98055, or SP600125, respectively.

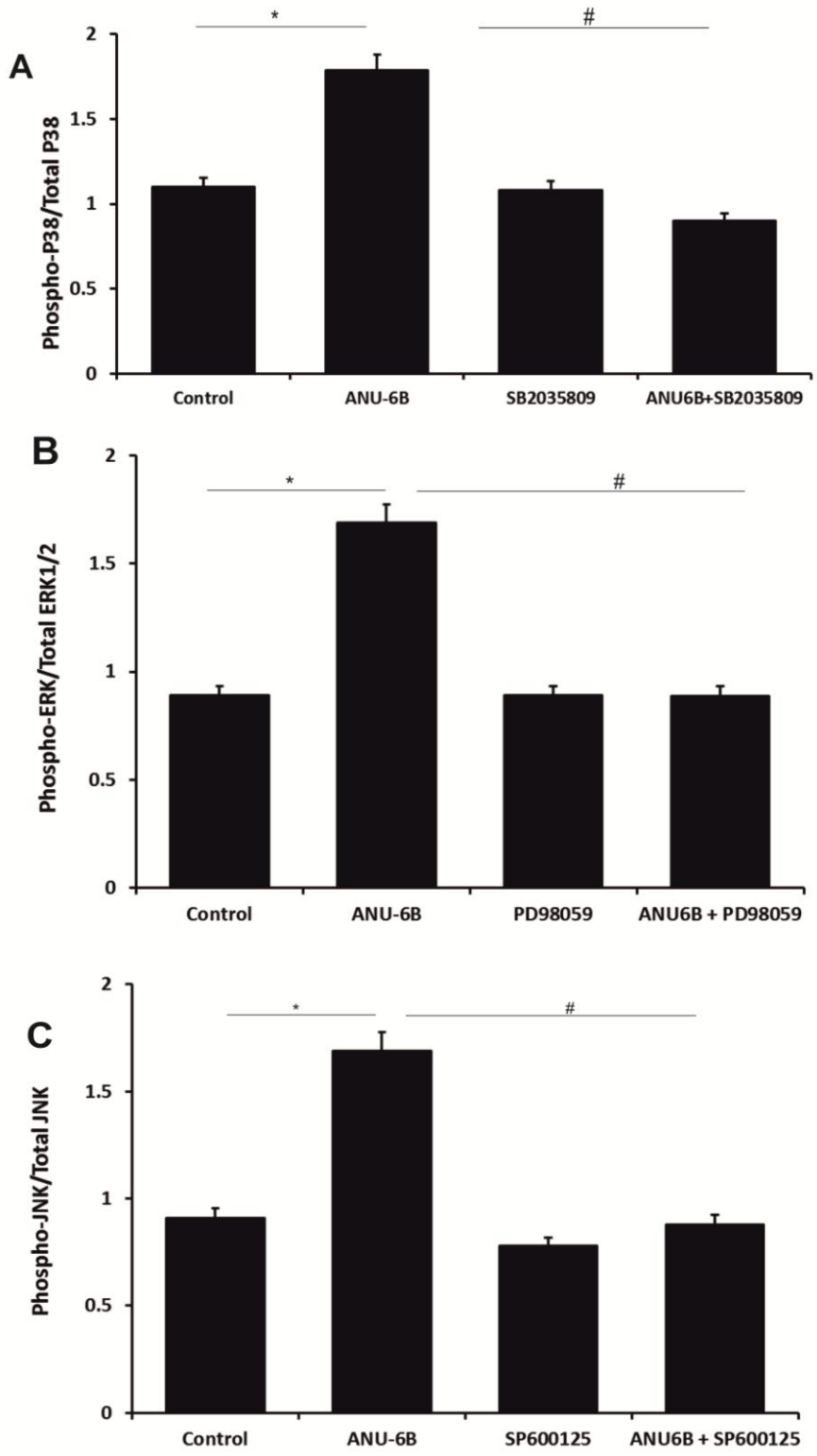

Figure 20: Effect of compound **14a** on activation of MAPK pathway in MCF-7 cells. **(A)** Phosphorylation of P38, **(B)** ERK1/2, and **(C)** JNK was determined by cell-based ELISA and expressed as the ratio of the phosphorylated to the total form of each protein. n=3 and **P*<0.0001 vs. control and $^{\#}P$<0.0001 vs. compound **14a** in the presence of SB2035809, PD98055, or SP600125, respectively.

3 Experimental section

3.1 General

All chemicals, salts, reagents and solvents were purchased from AVRA laboratories, Hyderabad, India; Aldrich (USA) and Alfa Aesar (USA). Reaction progress were observed by Thin Layer Chromatography plates. NMR (^{1}H &^{13}C) spectral data were obtained from 400 MHz Gemini Varian-VXR-unity instrument. Chemical shifts (δ) values are mentioned in ppm. Mass ESI spectra were taken from Micromass, Quattro LC using ESI+ software with capillary voltage 3.98 kV and ESI mode positive ion trap detector. Melting points were taken from an electrothermal melting point apparatus.

*3.2 Synthesis of bis(indolyl) hydrazide-hydrazone derivatives **14(a-d)***

1.86 mmol 1-methyl-indolyl-3-carbohydrazides **12a or 12b** were soluble in 3 mL Glac. CH_3COOH. To this 1.86 mM indole-3-aldehydes were added and allowed for heating at 90 °C over 6 h time period. Later the reaction mixture was neutralized by a cold $NaHCO_3$ solution. Further it was filtered and purified by recrystallization technique from ethanol then gave yellow color solid.

*3.2.1 5-bromo-1-methyl-N'-[(E)-(1-methyl-1H-indol-3-yl)methylidene]-1H-indole-3-carbohydrazide **14(a)*** Yield: 90%; m.p.: 233-235 ^{o}C; IR (KBr): 3439, 2916, 1627, 1523, 1462, 1370, 1285, 846, 744 cm^{-1}; ^{1}H NMR (DMSO-d$_6$, 400 MHz): δ 3.83 (s, 3H), 3.91 (s, 3H), 7.28-7.20 (m, 2H), 7.41 (s, 1H), 7.55-7.50 (m, 2H), 7.84 (s, 1H), 8.46-8.16 (m, 4H), 11.10 (brs, NH) ppm; HRMS *m/z* calculated for $C_{20}H_{18}ON_4Br$: 409.06585 $(M+H)^+$; found *m/z*:409.06546 $(M+H)^+$.

*3.2.2 1-methyl-N'-[(E)-(1-methyl-1H-indol-3-yl)methylidene]-1H-indole-3-carbohydrazide **14(b)*** m.p.: 248-250 ^{o}C; Yield: 86%; IR (KBr): 3216, 2912, 1625, 1547, 1463, 1382, 1237, 831, 738 cm^{-1}; ^{1}H NMR (DMSO-d$_6$, 400 MHz): δ 3.88 (s, 6H), 7.26 (s, 4H), 7.52 (s, 2H), 7.78 (s, 1H), 8.46-8.23 (m, 4H), 11.06 (brs, NH) ppm; HRMS *m/z* calculated for $C_{20}H_{19}ON_4$: 331.15534 $(M+H)^+$; found *m/z*: 331.15482 $(M+H)^+$.

3.2.3 5-bromo-N'-[(E)-(1H-indol-3-yl)methylidene]-1-methyl-1H-indole-3-carbohydrazide ***14(c)*** Yield: 87%; m.p.: 278-280 ^{o}C; IR (KBr): 3377, 3148, 2982, 1745, 1673, 1544, 1460, 1379, 1242, 874, 789 cm^{-1}; ^{1}H NMR (DMSO-d$_6$, 400 MHz): δ 3.89 (s, 3H), 7.23-7.14 (m, 2H), 7.55-7.38 (m, 3H), 7.80 (s, 1H), 8.54-8.22 (m, 4H), 11.26 (brs, NH), 11.63 (brs, NH) ppm; HRMS *m/z* calculated for $C_{19}H_{16}ON_4Br$: 395.05020 $(M+H)^+$; found *m/z*: 395.05038 $(M+H)^+$.

3.2.4 5-bromo-N'-[(E)-(5-methoxy-1H-indol-3-yl)methylidene]-1-methyl-1H-indole-3-carbohyd razide ***14(d)*** Yield: 92%; m.p.: 249-251^{o}C; IR (KBr): 3368, 3146, 2986, 1686, 1544, 1383, 843, 752 cm^{-1}; ^{1}H NMR (DMSO-d$_6$, 400 MHz): δ 3.84 (s, 6H), 6.79 (s, 1H), 7.30 (m, 3H), 7.51 (s, 1H), 7.84-8.07 (m, 2H), 8.41-8.50 (m, 2H), 11.01 (brs, NH), 11.14 (brs, NH) ppm; HRMS *m/z* calculated for $C_{20}H_{18}O_2N_4Br$: 425.06076 $(M+H)^+$; found *m/z*: 425.06008 $(M+H)^+$.

3.3 Cell lines and treatment

Cancer cell lines including Human cervical cancer (HeLa; ATCC No. CCL-2), Human breast adenocarcinoma (MDA-MB-231; ATCC No. HTB-26), Human breast adenocarcinoma (MCF-7; ATCC No HTB-22), Human alveolar adenocarcinoma (A549; ATCC No. CCL-185), Human colon adenocarcinoma (SW-680; ATCC No. CCL-227), along with head and neck squamous cell carcinoma (HNSCC) cell lines such as human pharynx squamous cell carcinoma (FaDu; ATCC No. HTB-43), human pharyngeal carcinoma (Detroit-562; ATCC No. CCL-138) and human tongue squamous cell carcinoma (SCC-25; ATCC No. CRL-1628) and normal human embryonic kidney (HEK-293; ATCC No. CRL-1573) cells were used in the present study. Cells were preserved in DMEM medium containing 100 mg/ml streptomycin and 100 units/ml penicillin and supplemented with heat-inactivated 10% FBS (fetal bovine serum). All cultured cells were kept in a humidified atmosphere at 37°C with 5% CO_2. Doxorubicin (Sigma-Aldrich, Schnelldorf, Germany) was taken as a target positive (cytotoxic) control. DMSO concentration was very less that was not greater than 0.1% in overall experiments.

3.4 MTT assay

Cells were cultured until a confluence of 80%, trypsinized and were sent to a falcon tube followed by centrifugation at 3000 rpm over 5 minutes before they were diluted in growth medium and seeded into 96 well microtitre plate. Number of cells suspended in 100 μL growth

medium ranged from 10 000 to 20 000 cancer cell lines per well based on the type of cell line. Now the cancer cell lines were attached over 16 h time period. Cancer cells were washed with serum free RPMI (assay medium) twice before treatment with compound. Compound **14a** at concentrations ranging from 1-200 μM was added to the cells with 3 parallel runs for each concentration. Doxorubicin and assay medium were treated as positive and negative controls, respectively. Then cells were incubated over 4 h and 10 μL MTT was mixed to each well and incubated over 2 h, then 70 μL medium was carefully removed from each well and 100 μL isopropanol was added. The plates were gently mixed and the absorbance was measured. Final results were calculated using the mean of three experiments, each with triplicate wells. The absorbance was found at 590 nm, and the amount of formazan in each well was directly proportional with the amount of living cells. The living cancer cell lines percentage was calculated by using the below equation.

Percentage of living cells = (A of treated cells – A of positive control)/ (A of negative control – A of positive control) × 100, where A is the absorbance.

3.5 Annexin V apoptosis assay

Prior to treatment, MCF-7 and HeLa cells were plated in 1 mL aliquots in a 24 well plate at 500,000 cells/well in three triplicates of each concentration. Cancer cell lines were reacted with 1 μL of a 1 μM DMSO stock solution of compound **14a**. The cells were incubated over particular period of time (8, 12 and 16 h) and these were then stained with propidium iodide (PI) and Annexin V-FITC. After respective tretments, cells were cleaned with PBS and these cells were resuspended in 10 mM HEPES, pH = 7.4, 2.5 mM $CaCl_2$, 140 mM NaCl, and 0.1% BSA (Annexin V binding buffer). Cells were incubated for 40 minutes time period with 5 μL FITC-annexin V conjugate, and then these cells were treated with 10 μL of 50 μg/mL PI and these were analyzed for cellular FITC and PI fluorescence was achieved by flow cytometry immediately.

3.6 Cell cycle distribution assay

24 well plates were used to seeded the MCF-7 and HeLa cells at 1 million cells/mL and were grown until upto they were 70% confluent. Cancer cell lines were reacted with compound **14a** (1 μM) and incubated for 16 h. Cold PBS was used for washing the harvested cancer cells

and processed for cell cycle analysis. Briefly it can say that, all the cancer cell lines were fixed in absolute ethanol and allowed for storing at –20 °C for further analysis. These fixed cancer cell lines were undergo centrifuged at 5,000 rpm speed and these cells were washed with cold PBS twice. RNase A (20 μg/mL final concentration) and propidium iodide staining solution (50 μg/mL final concentration) were allowed for adding to the above cancer cells and incubated at 37 °C over 30 min time period in the dark atmosphere. The cancer cell lines were analyzed by using FACS Calibur system (BD Biosciences, San Jose, CA, USA) interfaced with CellQuest 3.3 software. The results are indicated as the percentage of cancer cell lines in various phases of the cell cycle.

3.7 Measurement of intracellular ROS

The production of intracellular ROS in MCF-7 and HeLa cells was measured using DCFH-DA (2,7-dichlorodihydrofluorescein diacetate) assay (Wang and Joseph, 1999). The DCFH-DA is a non-fluorescent compound which is oxidized by ROS to form a cell permeable, fluorescent compound, 2, 7-dichlorofluorescein (DCF) that is measured at 520 nm. The assay was used to monitor the induction of intracellular ROS from MCF-7 and HeLa cells. These cell lines were cultured in 24-well plate at a particular density of 2×10^6 cells/well for 12 h, and were treated with compound **14a** at concentrations 1, 5 and 10 μM, along with tertiary butyl peroxide (t-BHP, 10 μM) as positive control. These cancer cell lines were incubated over 4 and 8 h and then 10 μM of DCFH-DA was adding to each well and then incubated over 10 min at 37°C. Then the cell lines were washed twice with PBS and the intracellular ROS accumulation was quantified by measuring the absorbance at 485 nm excitation and 520 nm emission wavelengths with the help of fluorescence spectrophotometer (Model F4500, Hitachi High Technologies Corp., Tokyo, Japan). To investigate the role of ROS in compound **14a** induced cell death and apoptosis, N-acetylcysteine (NAC, 5 mM), used as a ROS inhibitor was added to culture medium prior to the treatment with compound **14a**.

3.8 Measurement of nitric oxide production

The NO (nitric oxide) production in both HeLa and MCF-7 cancer cell lines was measured using Griess reagent assay (Zhang et al., 2004). These cancer cell lines were cultured in 24-well plate at a particular density of 2×10^6 cells $well^{-1}$ for 12 h. Then the cell lines were

reacted with compound **14a** at concentration levels of 1, 5 and 10 μM and allowed for incubation over 8 h time period at 37°C. Then the culture supernatant was collected and 100 μL of Griess reagent containing 0.002% N-1-naphtyl-ethylenediamine dihydrochloride, 0.5% sulfanilic acid and 14% glacial acetic acid was added. The NO generated in the culture supernatant was quantified by calculating the absorbance of the reaction mixture at 550 nm.

3.9 Kinase inhibition assay

The ability of compound **14a** to inhibit the phosphorylation activity of ABL (tyrosine kinase ABL) and PKA (cAMP-dependent protein kinase A) kinases was calculated by incubating them with the above compound at concentration levels of 1, 5, 10 and 50 μM. Here, kinase inhibition extent was calculated by using Kinase Reaction Rate Kit (BioThema, Haninge, Sweden). Phosphorylation inhibition was calculated by monitoring ATP degradation based on bioluminesence using staurosporine as positive control. Light emission was calculated after 5 min and 1 h time period from 96-well microtitre plate samples using an Envision Luminescence reader (PerkinElmer, Waltham, MA, USA). These values determined the data expressed as the percentage kinase inhibition.

3.10 PTP1B inhibition assay

The inhibition of protein-tyrosine phosphatase 1B (PTP1B) by compound **14a** was monitored with 6,8-difluoro-4-methylumbelliferyl phosphate (act as fluorogenic substrate) and recombinant human PTP1B (Merck-Calbiochem, Darmstadt, Germany). This assay buffer consisting of 50 mM sodium chloride (Merck), 25 mM HEPES sodium salt, 2.5 mM ethylene diaminetetraacetic acid disodium salt dehydrate, 2 nM 1,4-dithiothreitol (VWR), and 0.01 mg/mL human albumin. 52 to 210 μM test concentrations were generated by diluting the compound **14a** in 25 μL of assay buffer and it was added with 50 μL PTP1B soluble in assay buffer to afford 1.56 ng enzyme/well in black 96-well plates. Each concentration was performed for testing in three times (triplicate). After incubation over 30 min time period in the dark atmosphere then 25 μL of 10 μM DiFMUP solution was added. The fluorescent signal was measured using DTX 880 Multimode Detector (Beckman Coulter) at 10 min incubation in the dark followed by excitation and emission wavelengths of 360 nm and 465 nm respectively. The PTP inhibitor IV (Merck-Calbiochem) (0.16 mM concentration) was treated as positive control

and assay buffer also treated as the negative control. The results were shown as the percentage of inhibition in comparison to positive and negative controls.

3.11 Measurement of mitochondrial membrane potential

Rhodamine 123 was used to monitor the mitochondrial membrane potential. Cells were treated with the test compound **14a** at final concentration of 5 µM at different time intervals. Rhodamine 123 (final concentration 10 mM) was added to the cancer cell lines primarly and further these cell lines were harvested and incubated for 30 min at 37°C. Finally, these cell lines were collected, washed with PBS and analyzed by using FACScan Flow Cytometer and CellQuest software (Becton Dickinson). A lipophilic fluorone dye, Rhodamine 123 was selectively absorbed into mitochondrial membrane in live cells. Whenever the loss of mitochondrial membrane potential cannot be absorbed the rhodamine 123 into membrane.

3.12 Western blot analysis

HeLa and MCF-7 cell lines were reacted with compound **14a** at concentrations 1 µM, 3 µM and 5 µM and these cell lines were incubated over 24 h time period at a temperature of 37 °C. After the respective treatments, cells (10^6 cells/mL) were harvested. Total cell pellets were washed with PBS twice, lysed in ice-cold lysis buffer (150 mM NaCl, 50 mM Tris, 1% Triton X-100, 1 mM EDTA, 1 mM EGTA, 1 mM PMSF, pH 7.4, 10 mg/mL aprotinin, 10 mg/mL leupeptin, 1 mM sodium orthovandate and 1 mM NaF) over 30 min. time period and subsequently centrifuged at 13,000 rpm at 4°C for 30 min. Cell pellets were lysed in buffer A (10 mM HEPES, 10 mM KCl, pH 7.9, 1.5 mM $MgCl_2$, 0.5 mM DTT, 0.2 mM PMSF, dH_2O) for the extraction of nuclear protein. After incubation of cell lines on ice over 15 min then undergo centrifuged at 2,000 rpm at 4 °C over 3 min time period and the pellets were washed with buffer B (50 mM NaCl, 25% glycerol, 10 mM HEPES, pH 7.9, 0.1 mM EDTA, dH_2O). Finally, the pellets were resuspended in buffer C (420 mM NaCl, 25% glycerol, 20 mM HEPES, pH 7.9, 1.5 mM $MgCl_2$, 0.5 mM DTT, 0.2 mM EDTA, 0.2 mM PMSF) over 20 min on ice and allowed for centrifugation at 13,000 rpm at 4 ºC for 30 min time period. Protein content was quantified by using BCA Protein Assay Kit (Thermo Scientific, Rockford, IL, USA). For Western blot analysis, electrophoresis was used to separate the protein and changed onto a nitrocellulose membrane. Then the membrane was blocked by using non-fat milk for 1 h time period and

incubated with primary antibody such as caspase-3, -6, -7, -8, -9, Bcl2, BAK, Bid, Mcl-1 long, Mcl-1 short, actin primary antibodies in PBS at 4 ºC overnight. The membrane was cleaned with PBST (0.1% Tween 20 in PBS) on the next day and allowed for incubated with secondary antibody over 1 h at 28^{o}C. Then the membrane was again cleaned with PBST and finally the signal was discovered with an increased chemiluminescence detection kit (Amersham, Buckinghamshire, UK).

3.13 Detection of reactive oxygen species

Reactive oxygen species generated within HeLa and MCF-7 cells upon treatment with compound **14a** was evaluated using DCFDA fluorogenic assay. In the study, 5-(and-6)-chloromethyl-2′,7′-dichlorofluoresceindiacetateacetylester (CM-H2DCFDA, Invitrogen) act as fluorogenic molecular probe and was used for the quantification of intracellular reactive oxygen species. In independent experiments, HeLa and MCF-7 cells were cultured at a density of 2×10^6 cells well^{-1} in 6-well plates. Then the cells were reacted with compound **14a** at a last concentration of 5 µM and incubated over time period of 12 and 24 h at 37 ºC in a humidified CO_2 incubator. After the incubation, cells were harvested, cleaned with PBS and further incubated with 7.5 µL CM-H2DCFDA prepared in PBS for 30 min at 37 ºC. Then the cells were cleaned with ice-cold PBS and the ROS (reactive oxygen species) was monitored by analyzing fluorescence on a Becton Dickinson FACScan instrument (BD Biosciences Pharmingen, SanDiego, CA, USA) fitted with a 488 nm Argon laser.

3.14 Acetylated and total p53 sandwich ELISA assay

ELISA (Enzyme linked immunosorbent assay) was used to specifically evaluate the generation of endogenous levels of total and acetylated p53 protein in HeLa and MCF-7 cell lines. Briefly, in independent experiments, cells were reacted with 5 µM of compound **14a** and incubated for 12, 24 and 48 h. The acetylated and total p53 levels in treated and untreated cells was detected using ELISA Kit (Cell Signaling Technology). After treatment with compound **14a** for respective time periods, the cells were harvested, processed for protein extraction. Initially, the medium was removed from the cells, rinsed with very cold PBS and then lysed with 0.5 mL of ice-cold Cell Lysis Buffer with 1 mM PMSF. Cells were incubated on ice over 5 min and scraped off and transferred to an appropriate tube and a freeze-and-thaw cycle was performed

three times to further disrupt the cell membrane. These tubes were then centrifuged over 10 min time period at 4 °C and the supernatant was changed to a new tube. This supernatant was the cell lysate and was used for the ELISA and protein assays. Sandwich ELISA for acetylated and total p53 in HeLa and MCF-7 cells was performed according to the manufacturers' protocol. The absorbance of the plates was measured using an ELISA reader (Hyperion, Germany) at 450 nm. The results were expressed in terms of control index where the absorbance of each sample was divided by the absorbance of the untreated cell with the same incubation time. The results were determined as the average of independent triplicate experiments.

3.15 Determination of MAPK activation in MCF-7 and HeLa cells

The effect of compound **14a** on the phosphorylation of MAPK isoforms such as P38, JNK and ERK1/2 as indicative of MAPK activation was decided using cell-based ELISA kits (Ray Biotech Inc, Norcross, GA, USA.) as per manufacturer's instructions. Briefly, in independent experiments, HeLa and MCF-7 cells (20×10^3) were cultured and incubated in 96 well-plates overnight at 5% CO_2, 37^{o}C . Cells were reacted with 5 μM of compound **14a** and after incubation period, the cells were blocked and fixed. Then the cells were incubated with rabbit anti-total and phosphorylated P38 (p-P38), JNK (p-JNK) and ERK1/2 (p-ERK1/2) at 1∶100 dilution in the blocking solution, followed by HRP-conjugated mouse anti-rabbit IgG. Finally, 3, 3′, 5, 5′-Tetramethylbenzidine (TMB) was mixed, followed by optical density and stop solution was read at 450 nm by Spectra Max M2 spectrophotometer (Molecular Devices). The experimental results were showed as the ratio of the phosphorylated to the total form of each isoform protein. The results were indicated as the average of three independent experiments.

3.16 Statistical analysis

Experiments were conducted in three times (triplicate) and are showed as means ± SD of at least three experiments. Data were analyzed with (ANOVA) one-way analysis of variance followed by Bonferroni multiple comparisons and Bonferroni correction (P-values adjustment), and $P<0.05$ was treated statistically significant.

4 Conclusion

The compound **14a** exhibited anticancer activity by inducing apoptotic cell death via caspase independent pathway. Compound **14a** induced apoptosis via caspase independent pathway through the participation of mitogen-activated protein kinases (MAPK) such as extracellular signal related kinase (ERK) and p38 as well as p53 pathways. The human cancer cell lines MCF-7 and HeLa were used in the study. In both cell lines, compound **14a** induced the activation of pro-apoptotic proteins Bak and Mcl-1s in a caspase independent pathway during apoptotic cell death. Additionally, compound **14a** strongly induced the generation of reactive oxygen species which induced apoptosis by mediating the activation of various signal transduction pathways. In this study, we determined the pathways and mechanisms involved in compound **14a** induced apoptosis, namely the p53 pathways and MAP kinase cascades (p38, ERK and JNK MAPK). As a downstream target, p53 protein was activated and phosphorylated to induce p53-mediated cellular response. p53 protein interacted with MAPK (mitogen-activated protein kinase) pathways, including the SAPK/c-Jun N-terminal protein kinase (JNK) (stress-activated protein kinase), the p38 mitogen-activated protein kinase (MAPK), and ERK (extracellular signal related kinase). The results indicated that MAPK cascades p38 and p38 MAPK and ERK were indispensable for compound **14a** induced apoptotic activity in HeLa and MCF7 cell lines, since the adding of specific inhibitors of p38, ERK1/2 and JNK MAPK (SB2035809, PD98059 and SP600125) prevented the compound **14a** induced apoptosis. The current data clearly showed that MAP kinase cascades were necessary for apoptotic response to compound **14a** induced cellular killing and were dependent on p53 activity. In conclusion, this understanding of biochemical mechanisms and functional interaction with various signaling pathways triggered by compound **14a** in tumor cells (HeLa and MCF-7 cells) might provide new therapeutic strategies and reduce side effects and also may lead to the design and development of more efficient derivatives.

Acknowledgement:

The authors are thankful to CSIR, New Delhi, India for financial assistance in the form of Extramural Research Project with Scheme Number: 02(0114)/13/ EMR-II, Dated:12-04-2013.

References:

1. Hatti I, Sreenivasulu R, Jadav SS, Ahsan MJ, Raju RR. Synthesis and biological evaluation of 1,3,4-oxadiazole linked bis indole derivatives as anticancer agents. *Monatsh Chem.* 2015;146:1699–1705.
2. Hatti I, Sreenivasulu R, Jadav SS, Jayaprakash V, Kumar CG, Raju RR. Synthesis, cytotoxic activity and docking studies of new 4 – aza podophyllotoxin derivatives. *Med Chem Res.* 2015;24:3305–3313.
3. Ahsan MJ, K. Choudhary K, Jadav SS, Yasmin S, Ansari MY, Sreenivasulu R. Synthesis, antiproliferative activity and molecular docking studies of curcumin analogues bearing pyrazole ring. *Med Chem Res.* 2015;24:4166–4180.
4. Reddy NB, Burra VR, Ravindranath LK, Sreenivasulu R, Kumar VN. Synthesis and biological evaluation of benzoxazole fused combretastatin derivatives as anticancer agents. *Monatsh Chem.* 2016;147:593–598.
5. Reddy NB, Burra VR, Ravindranath LK, Kumar VN, Sreenivasulu R, Sadanandam P. Synthesis and biological evaluation of benzimidazole fused ellipticine derivatives as anticancer agents. *Monatsh Chem.* 2016;147:599–604.
6. Sreenivasulu R, Sujitha P, Jadav SS, Ahsan MJ, Kumar CG, Raju RR. Synthesis, antitumor evaluation and molecular docking studies of indole – indazolyl hydrazide – hydrazone derivatives. *Monatsh Chem.* 2017;148:305–314.
7. Madhavi S, Sreenivasulu R, Raju RR. Synthesis and biological evaluation of oxadiazole incorporated ellipticine derivatives as anticancer agents. *Monatsh Chem.* 2017;148:933–938.
8. Madhavi S, Sreenivasulu R, Jyotsna Y, Raju RR. Synthesis of chalcone incorporated quinazoline derivatives as anticancer agents. *Saudi Pharm J.* 2017;25:275–279.
9. Madhavi S, Sreenivasulu R, Ansari MdY, Ahsan MJ, Raju RR. Synthesis, biological evaluation and molecular docking studies of pyridine incorporated chalcone derivatives as anticancer agents. *Lett Org Chem.* 2016,13:682–692.
10. Agarwal M, Singh V, Sharma SK, Sharma P, Ansari MdY, Jadav SS, Yasmin S, Sreenivasulu R, Hassan MZ, Saini V, Ahsan MJ. Design and synthesis of new 2,5-disubstituted-1,3,4-oxadiazole analogues as anticancer agents. *Med Chem Res.* 2016;25:2289–2303.

11. Suzen S, Buyukbingol E. Anti-cancer activity studies of indolalthiohydantoin (PIT) on certain cancer cell lines. *Il Farmaco* 2000;55:246–248.
12. Buyukbingol E, Suzen S, Klopman G. Studies on the synthesis and structure-activity relationships of 5-(3'-indolal)-2-thiohydantoin derivatives as aldose reductase enzyme inhibitors. *Farmco (Societa Chimica Italiana)* 1994;49:443–447.
13. Suzen S, Buyukbingol E. Evaluation of anti-HIV activity of 5-(2-phenyl-3'-indolal)-2-thiohydantoin. *Il Farmaco* 1998;53:525–527.
14. Chen I, Safe S, Bjeldanes L. Indole-3-carbinol and diindolylmethane as aryl hydrocarbon (Ah) receptor agonists and antagonists in T47D human breast cancer cells. *Biochem Pharmacol.* 1996;51:1069–1076.
15. Kumar D, Sundaree S, Johnson EO, Shah K. An efficient synthesis and biological study of novel indolyl-1,3,4-oxadiazoles as potent anticancer agents. *Bioorg Med Chem Lett.* 2009;19:4492–4494.
16. Kumar D, Kumar NM, Sundaree S, Johnson EO, Shah K. An expeditious synthesis and anticancer activity of novel 4-(3'-indolyl)oxazoles. *Eur J Med Chem.* 2010;45:1244–1249.
17. Kumar D, Kumar NM, Chang KH, Shah K. Synthesis and anticancer activity of 5-(3-indolyl)-1,3,4-thiadiazoles. *Eur. J. Med. Chem.* 2010;45:4664–4668.
18. Kumar D, Narayanam MK, Chang KH, Shah K. Synthesis of novel indolyl 1,2,4-triazoles as potent and selective anticancer agents. *Chem Biol Drug Des.* 2011;77:182–188.
19. Hatti I, Sreenivasulu R, Jadav SS, Ahsan MJ, Raju RR. Synthesis and biological evaluation of 1,3,4-oxadiazole linked bisindole derivatives as anticancer agents. *Monatsh Chem.* 2015;146:1699-1705.
20. Giagoudakis G, Markantonis SL. Relationships between the concentrations of prostaglandins and the non steroidal anti-inflammatory drugs indomethacin, diclofenac, and ibuprofen. *Pharmacother.* 2005;25:18–25.
21. Brancale A, Silvestri R. Indole, a core nucleus for potent inhibitors of tubulin polymerization. *Med Res Rev.* 2007;27:209–238.
22. Singh P, Kaur M, Verma P. Design, Synthesis and anticancer activities of hybrids of indole and barbituric acids – Identification of highly promising leads. *Bioorg Med Chem Lett.* 2009;19:3054–3058.

23. Singh P, Kaur M, Holzer W. Synthesis and evaluation of indole, pyrazole, chromone and pyrimidine based conjugates for tumor growth inhibitory activities – Development of highly efficacious cytotoxic agents. *Eur J Med Chem.* 2010;45:4968–4982.

24. Gul W, Hamann MT. Indole alkaloid marine natural products: an established source of cancer drug leads with considerable promise for the control of parasitic, neurological and other diseases. *Life Sci.* 2005;78:442–453.

25. Bacher G, Nickel B, Emig P, Vanhoefer U, Seeber S, Shandra A, Klenner T, Beckers T. D-24851, a novel synthetic microtubule inhibitor, exerts curative antitumoral activity in vivo, shows efficacy toward multidrug-resistant tumor cells, and lacks neurotoxicity. *Cancer Res.* 2001;61:392–399.

26. Vicini P, Incerti M, Doytchinova IA, La Colla P, Busonera B, Loddo R. Synthesis and antiproliferative activity of benzo[*d*]isothiazole hydrazones. *Eur J Med Chem.* 2006;41:624–632.

27. Terzioglu N, Gursoy A. Synthesis and anticancer evaluation of some new hydrazone derivatives of 2,6-dimethylimidazo[2,1-*b*][1,3,4]thiadiazole-5-carbohydrazide. *Eur J Med Chem.* 2003;38:781–786.

28. Abadi AH, Eissa AAH, Hassan GS. Synthesis of novel 1,3,4-trisubstituted pyrazole derivatives and their evaluation as antitumor and antiangiogenic agents. *Chem Pharm Bull.* 2003;51:838–844.

29. Mohareb RM, Fleita DH, Sakka OK. Novel synthesis of hydrazide-hydrazone derivatives and their utilization in the synthesis of coumarin, pyridine, thiazole and thiophene derivatives with antitumor activity. *Molecules* 2010;16:16–27.

30. Gemma S, Kukreja G, Fattorusso C, Persico M, Romano MP, Altarelli M, Savini L, Campiani G. Synthesis of *N1*-arylidene-*N2*-quinolyl- and *N2*-acrydinylhydrazones as potent antimalarial agents active against CQ-resistant *P. falciparum* strains. *Bioorg Med Chem Lett.* 2006;16:5384–5388.

31. Dimmock JR, Vashishtha SC, Stables JP. Anticonvulsant properties of various acetylhydrazones, oxamoylhydrazones and semicarbazones derived from aromatic and unsaturated carbonyl compounds. *Eur J Med Chem.* 2000;35:241–248.

32. Sondhi SM, Dinodia M, Kumar A. Synthesis, anti-inflammatory and analgesic activity evaluation of some amidine and hydrazone derivatives. *Bioorg Med Chem.* 2006;14: 4657–4663.
33. Kucukguzel SG, Mazi A, Sahin F, Ozturk S, Stables J. Synthesis and biological activities of diflunisal hydrazide-hydrazones. *Eur J Med Chem.* 2003;38:1005–1013.
34. Garkani-Nejad Z, Ahmadi-Roudi B. Modeling the antileishmanial activity screening of 5-nitro-2-heterocyclic benzylidene hydrazides using different chemometrics methods. *Eur J Med Chem.* 2010;45:719–726.
35. Savini L, Chiasserini L, Gaeta A, Pellerano C. Synthesis and anti-tubercular evaluation of 4-quinolylhydrazones. *Bioorg Med Chem.* 2002;10:2193–2198.
36. Sirisoma N, Pervin A, Drewe J, Tseng B, Cai SX. Discovery of substituted *N'*-(2-oxoindolin-3-ylidene)benzohydrazides as new apoptosis inducers using a cell- and caspase-based HTS assay. *Bioorg Med Chem Lett.* 2009;19:2710–2713.
37. Ergenc N, Gunay NS, Demirdamar R. Synthesis and antidepressant evaluation of new 3-phenyl-5-sulfonamidoindole derivatives. *Eur J Med Chem.* 1998;33:143–148.
38. Zhang HZ, Drewe J, Tseng B, Kasibhatla S, Cai SX. Discovery and SAR of indole-2-carboxylic acid benzylidene-hydrazides as a new series of potent apoptosis inducers using a cell-based HTS assay. *Bioorg Med Chem.* 2004;12:3649–3655.
39. Jin L, Chen J, Song B, Chen Z, Yang S, Li Q, Hu D, Xu R. Synthesis, structure and bioactivity of N'-substituted benzylidene-3,4,5-trimethoxybenzohydrazide and 3-acetyl-2-substituted phenyl-5-(3,4,5-trimethoxyphenyl)-2,3-dihydro-1,3,4-oxadiazole derivati ves. *Bioorg Med Chem Lett.* 2006;16:5036–5040.
40. Vogel S, Kaufmann D, Pojarova M, Muller C, Pfaller T, Kuhne S, Bednarski PJ, Angerer Ev. Aroyl hydrazones of 2-phenylindole-3-carbaldehydes as novel antimitotic agents. *Bioorg Med Chem.* 2008;16:6436–6447.
41. Tantak MP, Klingler L, Arun V, Kumar A, Sadana R, Kumar D. Design and synthesis of bis(indolyl)ketohydrazide-hydrazones: Identification of potent and selective novel tubulin inhibitors. *Eur J Med Chem.* 2017;136:184–194.
42. Kumar D, Kumar NM, Ghosh S, Shah K. Novel bis(indolyl)hydrazide-hydrazones as potent cytotoxic agents. *Bioorg Med Chem Lett.* 2012;22:212–215.

43. Mukherjee DD, Kumar NM, Tantak MP, Das A, Ganguli A, Datta S, Kumar D, Chakrabarti G. Development of novel bis(indolyl)-hydrazide–hydrazone derivatives as potent microtubule-targeting cytotoxic agents against A549 lung cancer cells. *Biochemistry* 2016;55:3020–3035.
44. Ma Y, Yakushijin K, Miyake F, Horne D. A concise synthesis of indolic enamides: coscinamide A, coscinamide B, and igzamide. *Tetrahedron Lett.* 2009;50:4343–4345.
45. Sreenivasulu R, Durgesh R, Jadav SS, Sujitha P, Kumar CG, Raju RR. Synthesis, anticancer evaluation and molecular docking studies of bis(indolyl)triazinones, Nortopsentin analogs. *Chem. Pap.* 2017;72: https://doi.org/10.1007/s11696-017-0372-8.
46. James PN, Snyder HR. Indole-3-aldehyde. *Org Synth.* 1959;39:30.
47. Ishiyama H, Yoshizawa K, Kobayashi J. Enantioselective total synthesis of eudistomidins G, H, and I. *Tetrahedron* 2012;68:6186–6192.
48. Papayan GL, Galstyan LS. Indole derivatives. Amino esters of 1 – benzyl indole-3-carboxylic acids. *Arm Khim Zh.* 1976;29:1062–1064.
49. Whiting AL, Hof F. Binding trimethyllysine and other cationic guests in water with a series of indole-derived hosts: large differences in affinity from subtle changes in structure. *Org Biomol Chem.* 2012;10:6885–6892.
50. Jiang X, Tiwari A, Thompson M, Chen Z, Cleary TP, Lee TBK. A practical method for N-methylation of indoles using dimethyl carbonate. *Org Process Res Dev.* 2001;5:604–608.

Synthesis, antiproliferative and apoptosis induction potential activities of novel Bis(indolyl)hydrazide-hydrazone derivatives

Reddymasu Sreenivasulu,[1] Kotthireddy Thirumal Reddy,[1] Pombala Sujitha,[2] C. Ganesh Kumar,[2,*] and Rudraraju Ramesh Raju[1,*]

[1]*Department of Chemistry, Acharya Nagarjuna University, Nagarjuna Nagar – 522 510, Andhra Pradesh, India.*

[2]*Medicinal Chemistry and Pharmacology Division, CSIR-Indian Institute of Chemical Technology, Uppal Road, Tarnaka, Hyderabad 500007, Telangana, India.*

Graphicalabstract:

The target compounds cannot showed any cytotoxicity on normal HEK 293 kidney cell lines.

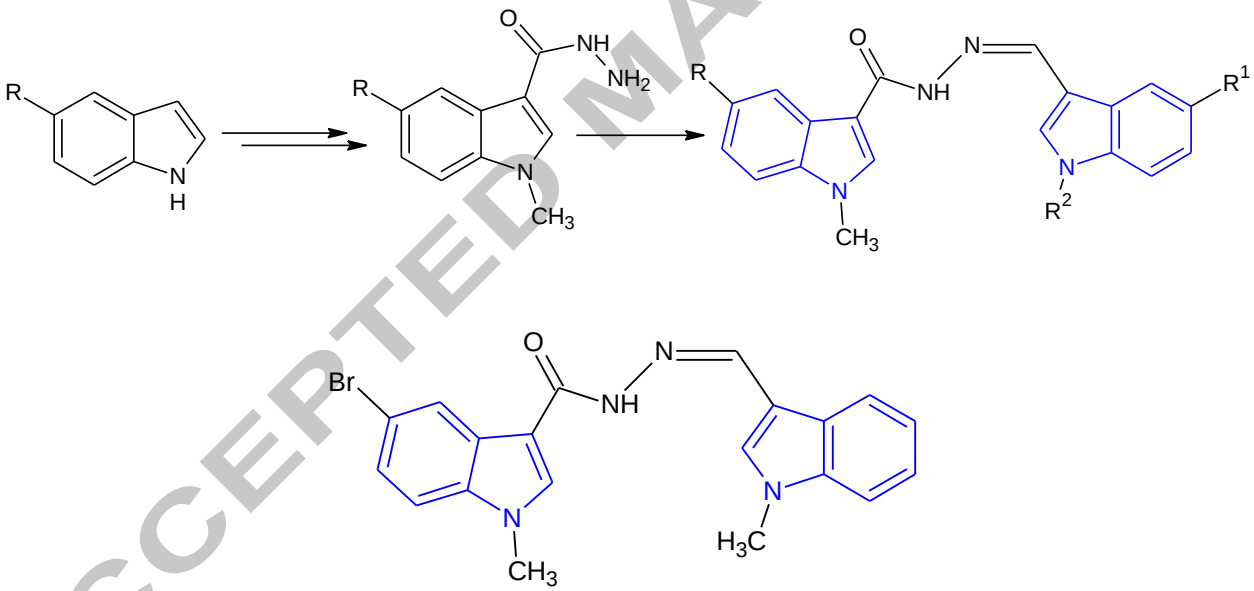

IC_{50} = 0.793 µM against A549